Universidad del País Vasco
Euskal Herriko Unibertsitatea

UNIVERSITÀ DEGLI STUDI DI MILANO BICOCCA

Bachelor Thesis in Physics

Spectroscopic study of galaxies in the Herschel Reference Sample.

Jon Fernández Otegi

Supervisors: **Giuseppe Gavazzi,**
Giuseppe Gorini
Supervisor at Home University: **Jon Urrestilla**

Academic Course 2014-2015

Contents

Chapter 1

Phenomenology of Galaxies

Galaxies are clusters of millions and billions of stars dynamically stable, with gas, dust and dark matter. They are the biggest isolated objects known in the Universe, with a diameter from 3 to 30 Kpc and a mass between 10^7 and 10^{12} $M_\odot$. Even though they are very complex systems, today we have a clear knowledge about their evolution and about their physical phenomena.
Aside from the stellar component there is a gaseous component, principally neutral Hydrogen (HI), and dust that, although is not a significant component in terms of the mass, plays an important role on the absorption phenomena. Finally, cinematic and other kind of observations suggest the existence of a spheric dark matter halo, dominant in terms of mass and more extensive than the barionic component.

1.1 Morphological Classification

In 1936 Edwin Hubble introduced a galaxy classification diagram based on their shape. This diagram, known as *Hubble Sequence*, is still used because of its simplicity and it divides galaxies in 3 classes: elliptical (early type), spiral (late type), and lenticular.

- The **elliptical galaxies**, indicated with the letter E, are galaxies with an ellipsoidal shape and are also divided in different subclasses depending on their eccentricity. This indicator can be obtained from $n = 10.\frac{a-b}{b}$, being a and b the mayor and minor axis of the galaxy respectively.

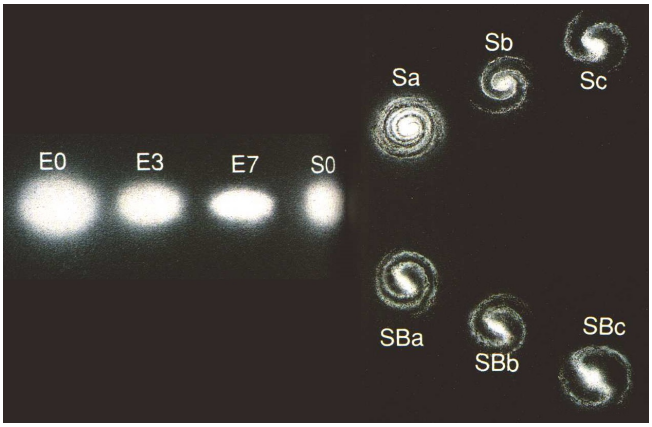

Figure 1.1: The *Hubble Sequence* is a galaxy classification diagram introduced by Edwin Hubble in 1936: on the right side, there are the spiral galaxies, on the left side the elliptical galaxies.

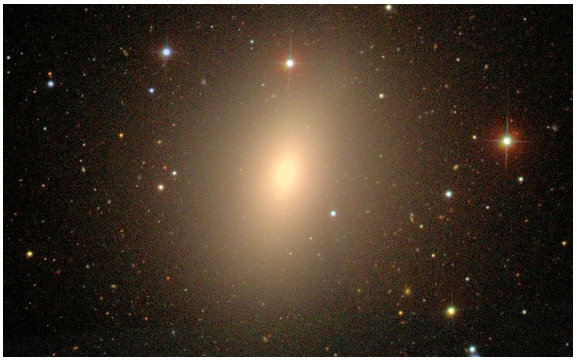

Figure 1.2: The galaxy NGC 4621, a typical elliptical galaxy: there is no evidence of dust and gas but only the presence of red old stars.

These systems are populated by old and not massive stars, and have almost no gas or interstellar dust. Therefore the star formation rate is minimum. The motion of their stars is chaotic around a the mass center with a velocity of hundreds of km/s. The elliptical galaxies are not isolated systems, they are grouped in clusters of galaxies called *clusters of galaxies*.

- **Spiral galaxies** are composed by a nucleus in the center with a high star density, a ellipsoidal bulge around the nucleus with old stars and a disk with spiral arms composed by young stars. In the Hubble Sequence, spiral galaxies are divided in simple spiral S, and barred spiral SB which have a bar through the nucleus region. These classes are divided in 3 subclasses, indicated with the letters a, b or c based on the extension of the arms and the dimension of the central bulge.

Figure 1.3: On the left, the spiral galaxy M 100; on the right the barred spiral galaxy NGC 1300. Both galaxies are regions of star formation because of the presence of gas and dust.

They are rich of gas and dust and, consequently, have high star formation rate. The motion of the stars in the disk is also circular with velocities of hundreds of $km.s^{-1}$.

- **Lenticular galaxies**, or *S0*, are an intermediate class between spiral and elliptical. They have a compressed shape, a sort of bulge and a spiral-like disk, but with no arms and old star population.
  Recent studies have proved the presence of big amount of gas (mostly atomic and molecular Hydrogen), and dust next to the nucleus, which proves the presence of star formation region.

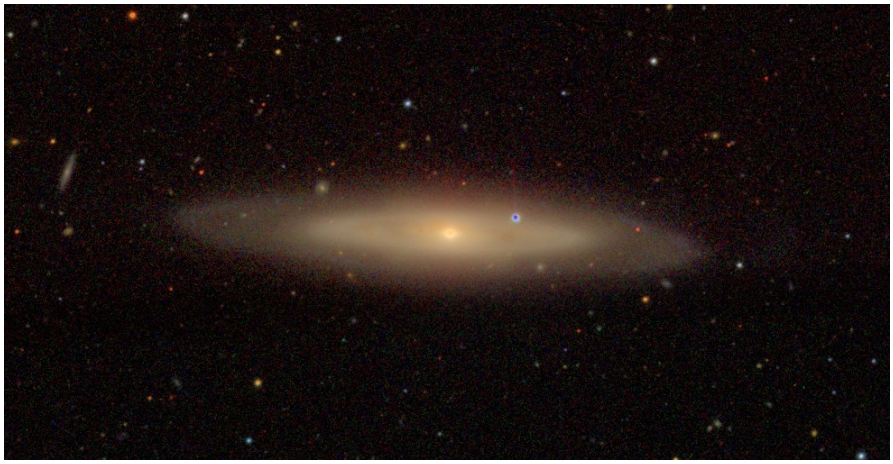

Figure 1.4: NGC 4866, a typical lenticular galaxy.

The Hubble Sequence doesn't take in account a very important class, the **Irregular galaxies**, so called because their not defined shape. These galaxies have a high activity of star formation due to their abundant amount of gas and dust. They are classified with the letters *Sm* (magellanic spiral) or *Im* (magellanic irregular), depending on the level of irregularity.

Figure 1.5: The Small and the Large Magellan cloud, a duo of irregular dwarf galaxies orbiting our Milky Way galaxy.

In addition to the Hubble classification, astronomers have also included the sub branches *d* and *m*, in which the arms are more notable and there is no presence of bulge.
The De Vaucouleurs system for classifying galaxies is a widely used extension to the Hubble sequence, first described by Gerard de Vaucouleurs in 1959.
De Vaucouleurs argued that Hubble's two-dimensional classification of spiral galaxies based on the tightness of the spiral arms and the presence or absence of a bar did not adequately describe the full range of observed galaxy morphologies. In particular, he argued that rings and lenses are important structural components of spiral galaxies. To complete Hubble's scheme, he introduced a more elaborate classification system for spiral galaxies, based on three morphological characteristics *B*ars, *R*ings and *S*piral arms.

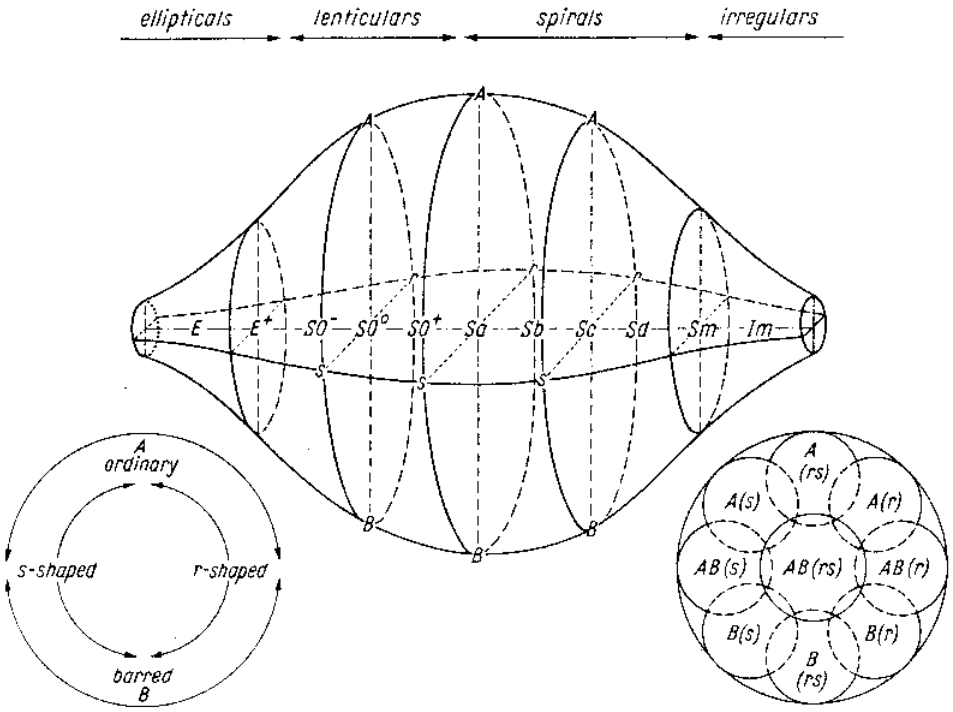

Figure 1.6: The de Vaucouleurs (1959) revised Hubble-Sandage classification system.

1.1.1 Properties of galaxies

The shape and the appearance of a galaxy are purely subjective evaluation criteria. Astronomers have been looking for objective characteristics that allow a classification based on measurable quantities.
First we study the radial profile of the light, i.e. the surface brightness dependence with the distance to the center the galaxy. The following are some of the most common profiles.

- **Sersic Profile**:

  Typical of the elliptical galaxies, is given by:

  $$I(r) = I_e e^{(\frac{r}{r_e})^{\frac{1}{n}}} \tag{1.1}$$

  I is the surface brightness in $mag.arcsec^{-2}$ at radius r, r_e the distance to the center containing the 50% of the emitted light and n the *Sersic Index*. The biggest and brightest systems have $n \geq 4$ while the nane ellipticals follow an exponential profile with *n=1*. The profile corresponding to *n=4* is called *Vaucouleurs Profile* and describe the most luminous galaxies dominated by a big bulge.

The *Sersic Index* controls the curvature of the profile: the small values indicate a minor contribute of the central region.

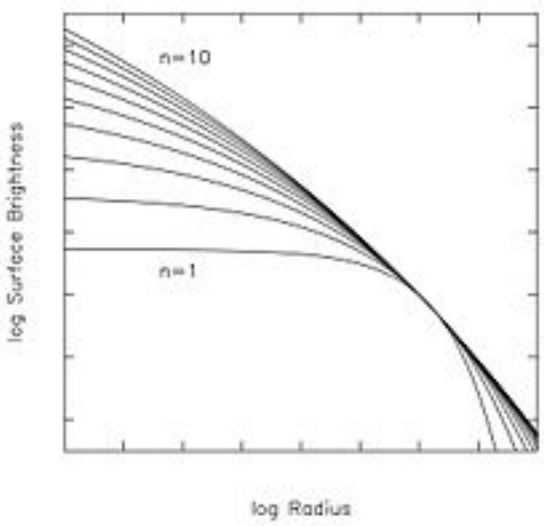

Figure 1.7: Sersic profile depending on the value of n.

- **Exponential Profile**:
  Describes disk galaxies without a large bulge.In this case surface brightness is proportional to e^r.

- **Mixed Profile**:
  It is a combination of the two previous profiles. It describes large spiral galaxies which containt a luminous bulge and extensive disc.

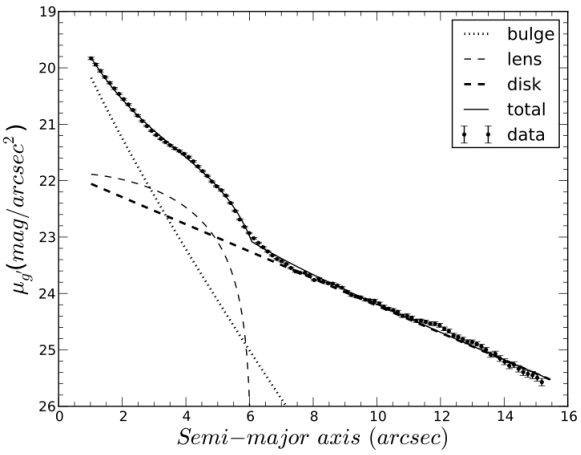

Figure 1.8: Example of mixed profile.

From the analysis of the this profile it's possible to obtain different parameters that allow us to classificate the galaxies:

- **Concentration Index**:
  Defined as $C_{31} = \frac{r_{75}}{r_{25}}$, where r_{75} and r_{25} are the radius containing the 75% and 25% of the total luminosity of the galaxy respectively. The bigger is this parameter, the more concentrated is the system, like on the elliptical galaxies. On the other hand the spiral galaxies have a lower concentration index.

- **Colour Index**:
  Gives the luminosity difference between two photometric bands and allow us to stimate the age of the star population. Typically the spiral galaxies are rich in young stars and, therefore, their color is more blue while the elliptical ones have a more red color.

The *Concentration Index*, *Color Index* and the luminosity of the H band, that allow us to stimate the stellar mass of the galaxies, are the minimum number of parameters required to characterize a galaxy. The *Color-Magnitude* diagram is a useful instrument that relates the color and the luminosity of the galaxies. In the figure (1.9) we can observe the Color-Magnitude diagram for the *Coma Bernices* supercluster.

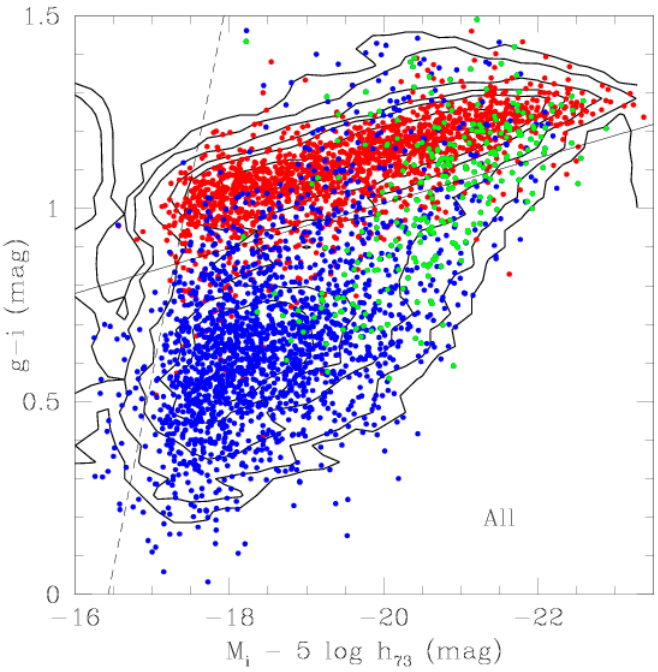

Figure 1.9: Color-magnitude diagram of the Coma Bernices.

The red points are used to represent Early Type galaxies, blue for the *Sc* and *Sd* and green for the *Sa* and *Sb*. Galaxies of different type occupate different regions: the *Red*

Sequence(occupied by the most early galaxies) and the *Blue Cloud* (occupied by the most late galaxies). The intermediate class of the Sa and Sb represents the contact point between the previous two zones. Consequently it is possible to deduce that the prominent bulges characterize the transition from the early galaxies to the late ones.

1.2 Spectral Energy Distribution

Spectral energy distribution (SED) is a plot of brightness or flux density versus frequency or wavelength of light. By combining the photometric information of different band of electromagnetic spectrum we can obtain the spectral energy distribution of a galaxy. This spectrum contains from radio wavelengths to the X or gamma rays. Each band is related to different components of the galaxy.

An example of SED is shown in the figure (1.10).

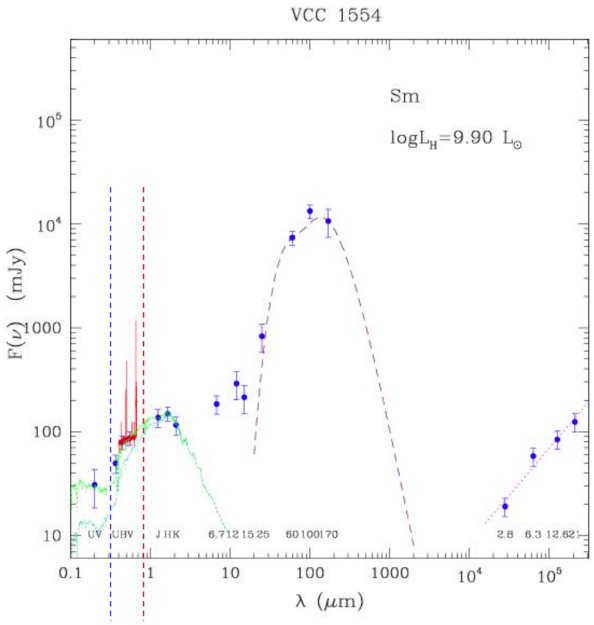

Figure 1.10: Spectral Energy Distribution of VCC-1554.

The first peak from the left represents the stellar component, which goes from the UV to the NIR. This part is compose by the stellar continuum and the emission-absorption lines of the stars. The second peak comes from the thermal emission of the dust and at the end we can observe the synchrotron emission in the Radio band.

1.2.1 Continuum Emission

Stars emit as a black body: a system in which the matter and the radiation are in thermal equilibrium. One of the most important properties of the black body radiation is that the wavelenght of peak of the spectrum depends on the temperatura following the *Wien Law*:

$$\lambda_{max} T = 0.29 \quad cm.K \tag{1.2}$$

Therefore the hottest stars ($\sim 10^4 K$) have the peak in the UV and the oldest ($\sim 10^3 K$) in the NIR. In a galaxy we observe an integrated luminosity of its stars so examining the UV, visible and NIR regions we can obtain information about the star population. In fact, in the elliptical galaxies and in the bulges of spiral galaxies, where cold and old star are dominant, have a spectrum with a peak in the NIR and the spiral and irregular ones have a bigger contribution in the UV region.

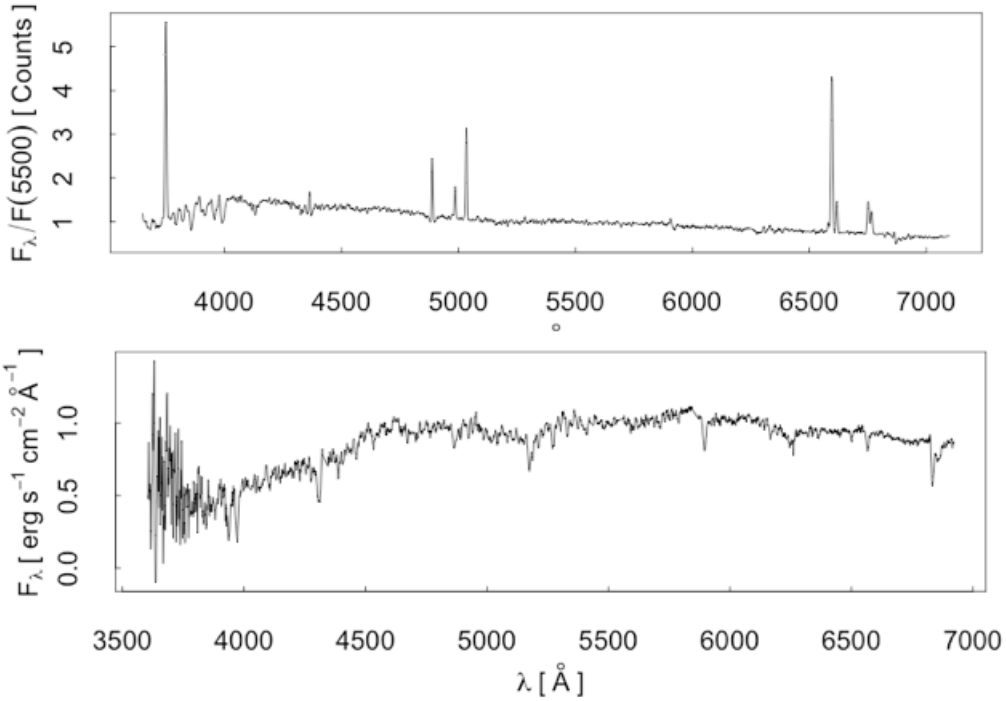

Figure 1.11: The spectrum at the top represents a typical spiral galaxy (HRS 275) and the one at the bottom is the spectrum of an elliptical passive galaxy (HRS 234). It is clear that the spectrum of the spiral galaxy is stronger in the blue because of its younger population of stars. The elliptical, instead, has its mayor contribution in the red region.

Interstellar dust can also be found in galaxies, specially the spiral and irregular types. This dust is constituted of heavy elements (metals) created on the stellar nucleosynthe-

sis.
The dust grains have different dimensions, forms and compositions. The *Big Grains* ($\sim 0.1\mu m$) absorb principally in the visible and IR, and are usually composed of carbon or silicates. They are also in thermal equilibrium with interstellar radiation at a temperature of 10-20 K and emit radiation at wavelenghts over 100 μm.
Very Small Grains (0.01 or less) are made of carbon and absorb in UV. They are so small that the incident photons heat them beyond the equilibrium temperature and make them emitbetween 20 and 100 μm.
There are also the so called *Policyclic Aromatic Hydrocarbons*. They also are ultraviolet absorbents and emit in the NIR region.

Finally, the emission at highest wavelenghts, in the Radio region, is due to synchrotron emission: relativistic electrons accelerated by supernova shock waves that lose their energy by interacting with the magnetic field of the galaxy.

Galaxies also emit in X-rays (1-100 Å). In this band emission is due to the accretion of binary systems or, in the AGN, to the falling of matter into the black hole.
Also the hot gas is a X-ray source the emission. The emission is created by electrons that are deflected because of the electric field of an ion inside of a very hot gas. This effect is called *Breemstrahlung*.

1.2.2 Emission Lines

The galaxy spectrum usually contains emission and absorption lines, overlapped to the continuum, due to energetic transitions inside the atoms or components of the interstellar medium.
The characteristics of the lines allow us to obtain information about the emitter. In fact, from the analysis of the line's wavelenght it is possible to trace the presence of atomic and molecular gas. The intensity of the line gives information about the abundance of the element.
In the end, from the line intensity and it's profile it is possible to study the kinematics of emitting species in the galaxy.

- **Atomic Hydrogen (HI)**
  The atomic neutral hydrogen can be easily mapped by the observation of the 21 cm line. When the spin of the electron and the proton are parallel the atom has slightly more energy than when they are antiparallel. This transition produces a photon with 21 cm wavelenght.

  Although this transitions occurs once in 10^7 years, the abundance of HI makes possible to observe the line. Therefore, the Hydrogen is can be trace on spiral and irregular galaxies, where there is a very big quantity of interstellar gas.

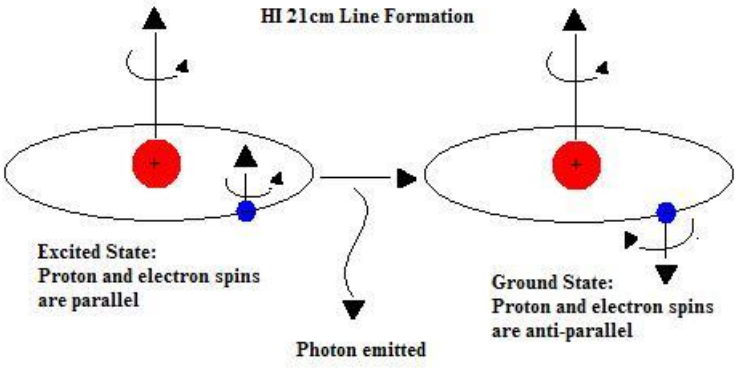

Figure 1.12: Illustration of the fine structure transition that produces the 21 cm line.

From the line intensity it is possible to calculate the amount of gas of the galaxy. The HI mass tipically goes from 10^8 to 10^{10} solar masses, which represents approximately the 10% of the total mass. The fraction of gas mass over the stellar mass decreases when increasing the total mass of the galaxy. In the most massive galaxies (like our Milky Way) it is around 10 % and for less massive around 100 %.

The spatial distribution of HI is more extended than the stellar disk, with a relative minimum on the central region. This distribution generates the typical double horn shape of the 21 cm line:

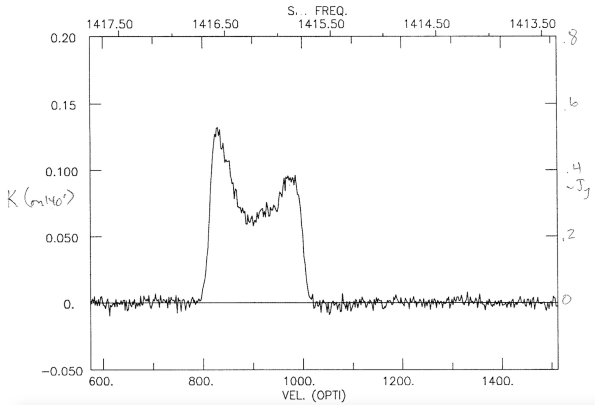

Figure 1.13: 21 cm line.

- **Hydrogen Molecule (H_2)**
  The direct observation of H2 is difficult (the temperature in the galaxy is not high enough to excite the rotational states of the molecule), so its presence is

inferred essentially from the CO tracer. The carbon monoxide is the most abundant molecule after H_2; its dipole moment is small and therefore CO can be easily excited. Its estimation can be carried out using a conversion factor that depends on the metallicity of the galaxy. The form of the molecular Hydrogen distribution is not very different from the one atomic hydrogen, confirming that their kinematic properties and spatial distribution is quite similar (even if the amount of molecular hydrogen is much lower).

- **Ionized Hydrogen (HII)**
  The dominating component of ionized gas is the HII. The HII region have temperatures of $\sim$ 8000 K and densities of 0.2-0.5 atoms cm^{-3} and is an indicator of star formation. The typical distribution of the HII is exponential, very similar to the stellar distribution.

Figure 1.14: Strings of the HII regions delineate the arms of the Whirpool Galaxy.

The gas is ionized by the UV photons emitted by the stars. When an electron goes from a state n_2 to another less energetic state n_1, emits a photon whose energy is the difference between the two levels:

$$E_\gamma = (n_2 - n_1)h\nu \tag{1.3}$$

The transitions from different excited states to the ground state are known as the *Lyman Series* and emit photons in the UV band. On the other hand, the Balmer series correspond to emissions of photons by electrons in excited states going to the second level, and these photons have optical wavelength. Particularly important is the transition from the third to the second level, which line (H_α, 6562,81 $\mathring{\text{A}}$) is very frequently measured. The transitions dropping in the 3rd and 4th orbitals are known as the Paschen and Brackett series, which lines can be observed in the IR.

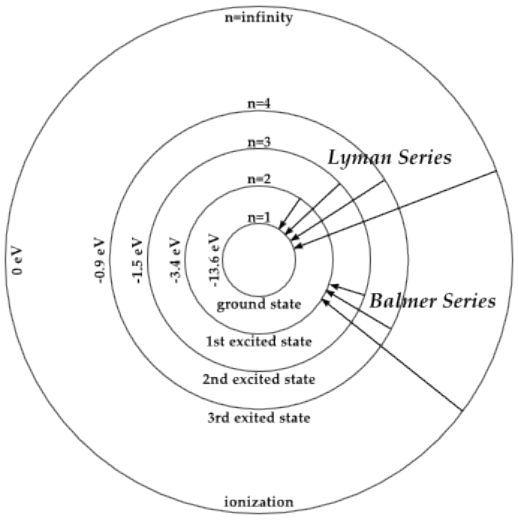

Figure 1.15: Energy levels and transition lines of the Hydrogen atom.

There are other important emission lines that are not produced by the hydrogen. For example, the $SII$is a partial indicator of supernovae's waves and the NII indicates the metallicity of the interstellar medium.

- **Absorption Lines**
  The absorption lines depend on physical parameters of the stars. These can be classified in different spectral types (O,B,A,F,G,K,M) depending on the type and intensity of the absorption lines in the visible part of the spectra. The absorption in this region depends on the temperature: the hottest stars produce absorption lines of the hydrogen (Balmer Series), and the colder the stars are the weaker this lines become and other absorption lines related to other elements appear.
  Their intensity depends on the age and metallicity of the star population. Intense lines are characteristic of old star populations: elliptical galaxies, lenticular galaxies or spiral's bulge.

The most important absorption lines are shown in the table (1.1).

Line	λ	**Indicator**
H δ	4101 Å	Age
D4000	4000 Å	Age and Metallicity
G_{4300}	4300 Å	Age
H_β	4861Å	Age
Mg_2	5156 Å and 5197 Å	Metallicity
Fe	5270 Å and 5335 Å	Metallicity
NaD	5879 Å and 5911 Å	Age and Metallicity

Table 1.1: Principal absorption lines of the galaxies.

1.3 Redshift and Distribution of galaxies

When observing the spectrum of a distant galaxy, it's lines are shifted to higher wavelenghts. This phenomena is called *Redshift*.
The Redshift is just a manifestation of the Doppler effect due to the expansion of the universe and is defined as:

$$z = \frac{\lambda_0 - \lambda_e}{\lambda_e} \tag{1.4}$$

Where λ_0 is the observed wavelenght and λ_e the emitted one.
In the 1929 Edwin Hubble studied the dependence between the redshift and the the distance to our galaxy, obtaining the famous linear relation known as the *Hubble Law*:

$$cz = H_0 D \tag{1.5}$$

Where H_0 is the Hubble constant. According to his estimation it's value should be around 500 $km.s^{-1}.Mpc^{-1}$, but more recent studies have shown that a more accurate result is:

$$H_0 = 73.8 \pm 5.0\ km.s^{-1}.Mpc^{-1} \tag{1.6}$$

It is possible to obtain the velocity between us and another galaxy from the redshift. However, this is not valid for galaxies forming a cluster. In fact, they follow random orbits around the center of the cluster. The distribution of velocities on such a cluster gives a gaussian from which peak we can obtain the preceding velocity of the cluster itself. It is also used to measure the mass of the cluster using the velocity dispersion of the gaussian and the virial theorem.

1.3.1 Distribution of galaxies in the Universe

This method to calculate the distance from the redshift has allowed to map the distribution of the galaxies in the universe. The galaxies are not uniformly distributed, they are mostly in groups of few tens of them or in rich cluster with hundred of galaxies.
The Milky Way is part of a group of galaxies called *Local Group*. In the Local Group there are two big galaxies (the Milky Way and M31), some intermediate galaxies (M33, M32, LMC and SMC) and loads of dwarf irregulars galaxies. In addition, it is moving to a big concentration of galaxies called *Virgo Cluster* and situated to 15 Mpc. The Virgo Cluster is composed of thousand of galaxies. At the center we can find elliptical and lenticular galaxies, but because of being still in formation, we can also find some spiral and irregular galaxies.

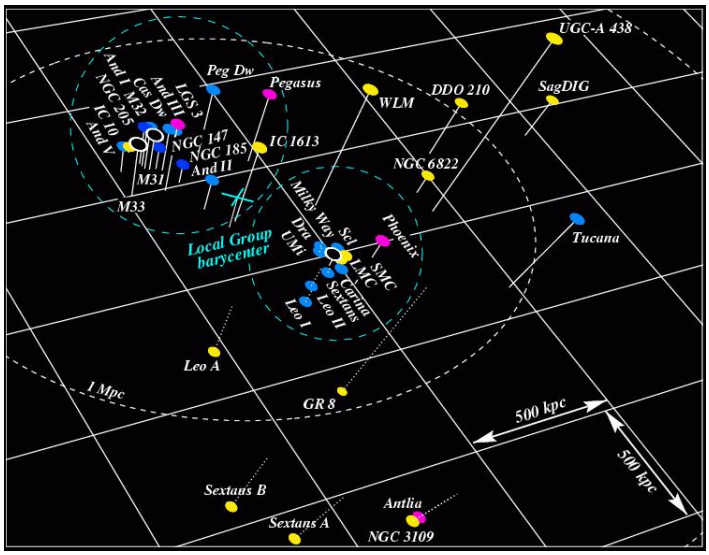

Figure 1.16: Distribution of the galaxies in the Local Group. The color of the galaxies indicate the morphologic type: black for spirals, blue for spheroidal nanes, yellow for irregular nanes and pink for intermediate between spheroidal and irregular galaxies.

The galaxy clusters have a radius of some Mpc, and the galaxies constitute about 10 % of the mass (20 % is intergalactic gas and 70 % dark matter). The intergalactic medium is composed by hot ionized gas ($\sim 10^6$ K) that emits X rays via Bremsstrahlung. The galaxies in the cluster have dispersion velocities of approximately 1000 km s^{-1} and the inclination and eccentricity of their orbits is random.

The Local Group and the Virgo cluster form the *Local Supercluster*. If we go further we find the *Coma Cluster*, which is much bigger than Virgo. Although if it is 100 Mpc far, it is three times more luminous than the Local Group. Most of it's galaxies are elliptical and lenticular.
The distribution of the galaxies at bigger scales has been recently investigated with

surveys as *2dFGRS* or *SDSS*.

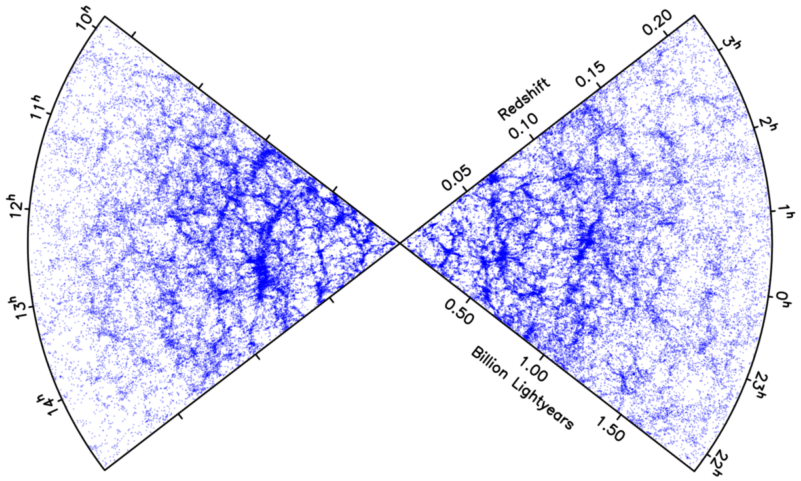

Figure 1.17: Distribution of galaxies obtained by 2dFGRS. We note that there are regions with high intensity (clusters) connected by regions with small quantities of objects (called Cosmic Vacuums).

1.4 Active Galactic Nuclei

Some galaxies have a Spectral Energy Distribution more extended than what is expected from a system composed of stars, gas and dust. These galaxies emit along the whole electromagnetic spectrum, from the Radio to the X rays, suggesting that this radiation is not thermal. In addition, in the visible and UV regions there are loads of intense emission lines.
This galaxies are called *active*, and the non-thermal emission comes from a central region (of few kpc) called *Active Galactic Nucleus* or *AGN*. One of the most remarkable characteristics of the AGN is it's huge luminosity in the X band, which can be 1000 times stronger than the one of a usual galaxy.
The emission of such a big amount of energy in such a small region suggests that it's produced by a compact and massive object. Nowadays it's accepted that this central source is a Super Massive Black Hole (SMBH) that emits due to accretion.

The understanding of the properties and the formation of an AGN is a very important part of the theory of the galactic evolution and formation. Almost all the spheroidal galaxy has a SMBH (not necessarily in accretion at present) and therefore most of the galaxies have have an active phase in the past, which have surely affect the evolution of the galaxy.

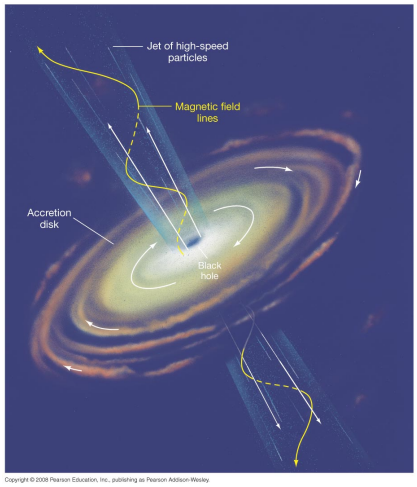

Figure 1.18: Representation of an active galaxy.

1.5 Spectrum Classification

There are two principal ways to classify the galaxies which differ in the number on emission lines taken into account:

1.5.1 WHAN Diagram

The *WHAN diagram* combines the equivalent width of $EH\alpha$ ($WH\alpha$) and the $[NII]/H\alpha$ equivalent width ratio in order to classify the ionization source(s) in galaxies.
From *Cid Fernandes et al. (2011)*, five classes of galaxies are identified within the *WHAN diagram*. Since the $H\alpha$ line is the result of a emission component due to the photoionization of HII region, and an absorption component due to the stellar atmospheres, there is a correction of its equivalent width according to *Gavazzi et al. (2011)*:

$$EW\ H\alpha_{corr} = EW\ H\alpha - 1.3 \tag{1.7}$$

Thus, the true conditions of *Cid Fernandes et al. (2011)* for all the types of galaxies, are the following:

1. **Pure star-forming galaxies**, with the so called **HII region**, in which the most present gas is the ionized hydrogen:

$$\log\Big(\frac{[NII]}{H\alpha_{corr}}\Big) < -0.3 \qquad\qquad |EW\ H\alpha_{corr}| > 1.5 \tag{1.8}$$

2. **Strong AGN** (i.e. *Seyferts*), galaxies with a supermassive black hole in their center and a powerful activity:

$$\log\Big(\frac{[NII]}{H\alpha_{corr}}\Big) > -0.3 \qquad\qquad |EW\ H\alpha_{corr}| > 6 \tag{1.9}$$

3. **Weak AGN**, galaxies with a supermassive black hole in their center and a less powerful activity than sAGN:

$$\log\left(\frac{[NII]}{H\alpha_{corr}}\right) > -0.3 \qquad 1.5 < |EW\ H\alpha_{corr}| < 6 \tag{1.10}$$

4. **RG** (*retired galaxies*) (i.e. *fake AGN*), old galaxies with a old stellar populations able to ionize the surrounding gas and produce spectra identical to those of AGN. So they are galaxies that cease their star forming activity:

$$0.5 < |EW\ H\alpha_{corr}| < 1.5 \tag{1.11}$$

$$|EW\ H\alpha_{corr}| < 0.5 \qquad |EW\ [NII]| > 0.5 \tag{1.12}$$

5. **Passive galaxies** (actually, *lineless galaxies*), with no activity:

$$|EW\ H\alpha_{corr}| < 0.5 \qquad |EW\ [NII]| < 0.5 \tag{1.13}$$

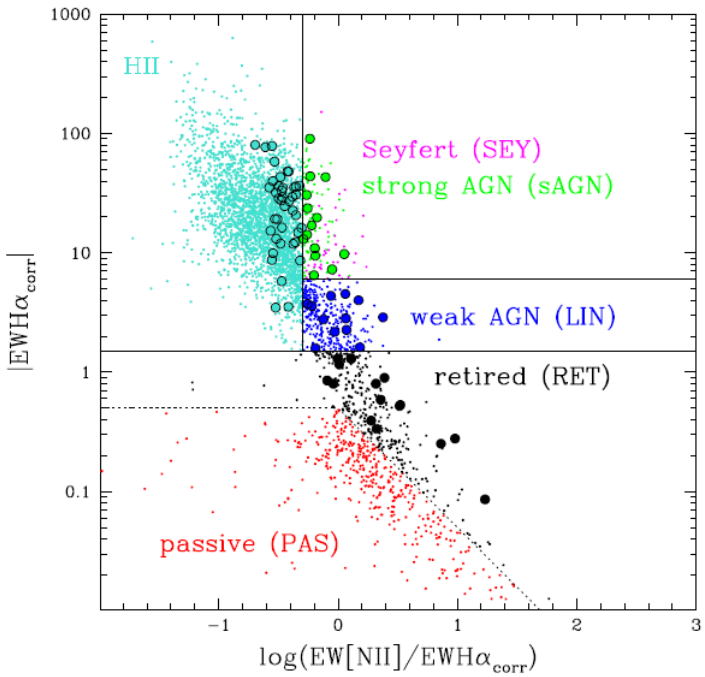

Figure 1.19: Example of WHAN diagram from *Gavazzi et al. (2011)*.

The following figures represent the typical shape of the spectrum of these kind of galaxies.

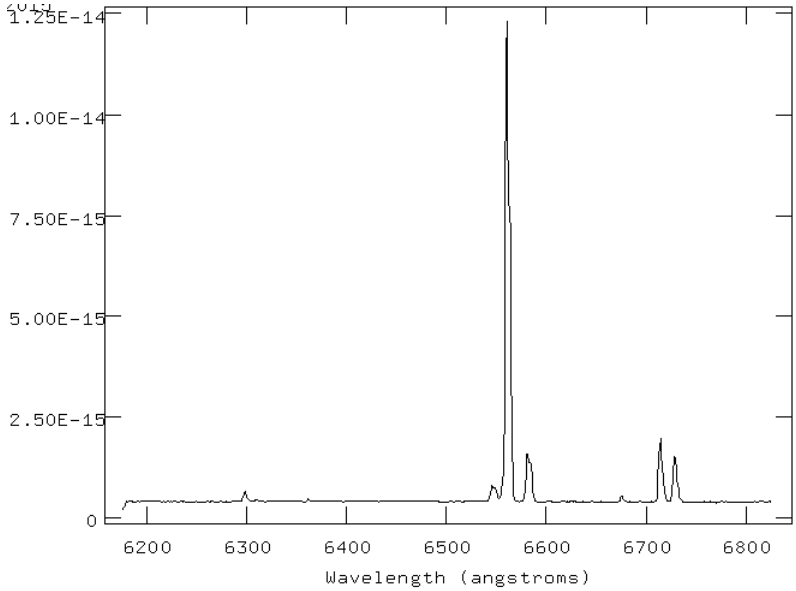

Figure 1.20: Combination of the spectrum of 10 HII Region galaxies taken from NED. Represents the typical shape of this type of galaxy in this range of wavelenghts.

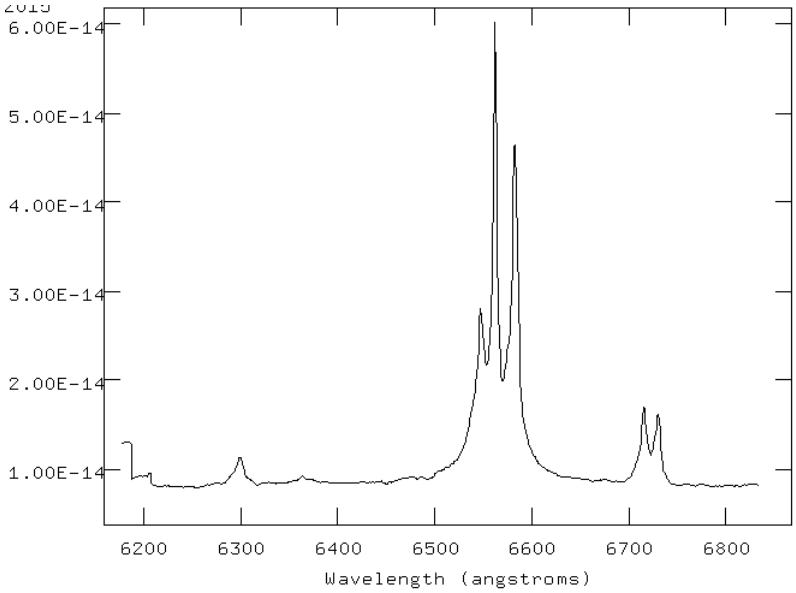

Figure 1.21: Combination of the spectrum of 10 Strong AGN taken from NED. Represents the typical shape of this type of galaxy in this range of wavelenghts.

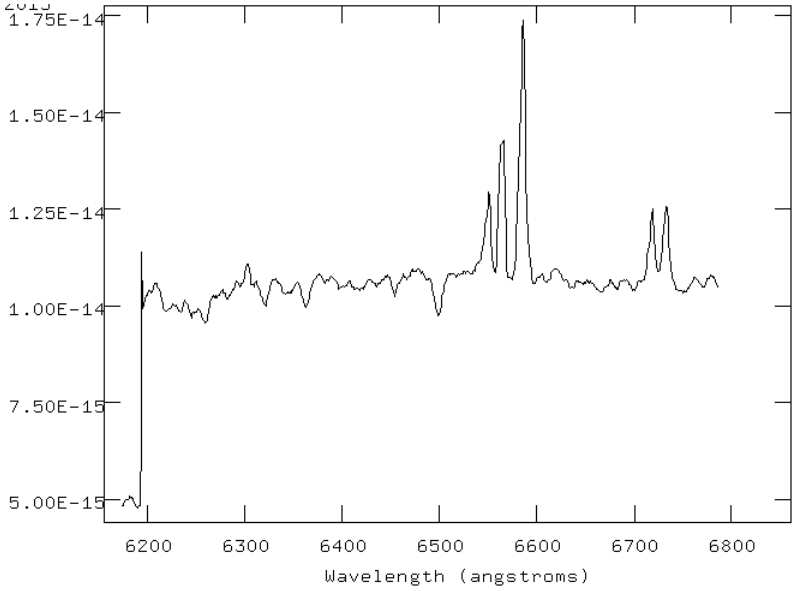

Figure 1.22: Combination of the spectrum of 10 Weak AGN taken from NED. Represents the typical shape of this type of galaxy in this range of wavelenghts.

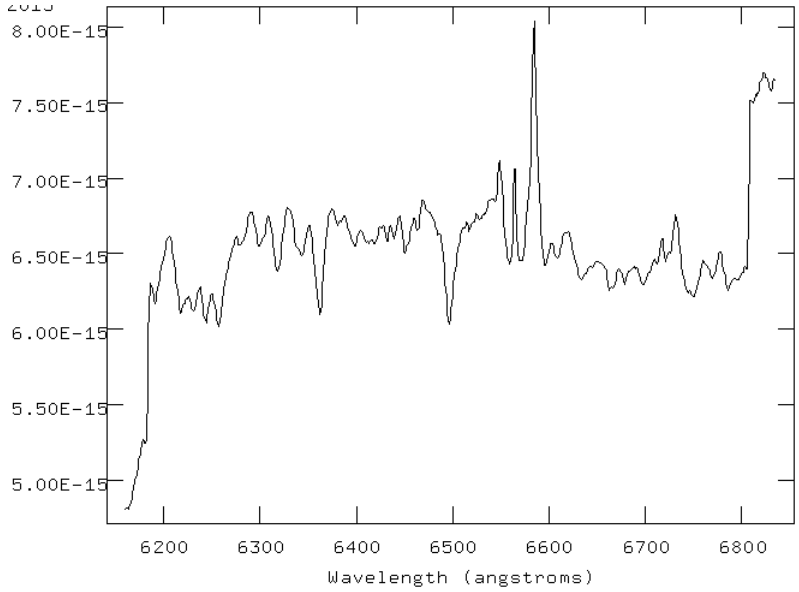

Figure 1.23: Combination of the spectrum of 10 Retired galaxies taken from NED. Represents the typical shape of this type of galaxy in this range of wavelenghts.

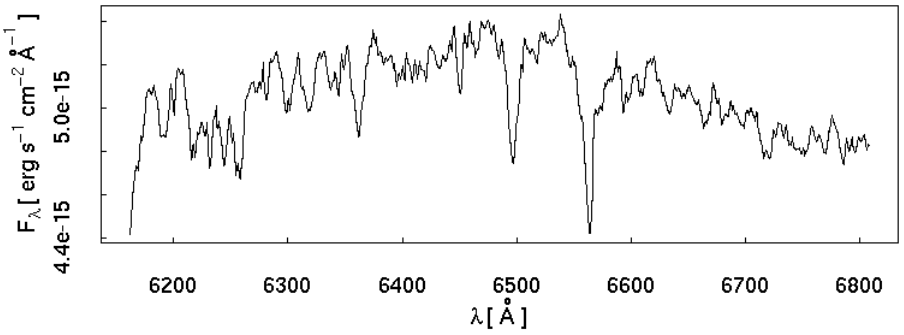

Figure 1.24: Spectrum of a passive galaxy taken from NED (HRS 234). Represents the typical shape of this type of galaxy in this range of wavelenghts.

1.5.2 BPT Diagram

The so called *BPT Diagram* (named after Baldwin, Phillips and Telervich) is a set of nebular emission line diagrams used to distinguish the ionization mechanism of nebular gas. The most famous version consists of $[NII]6583/H\alpha$ versus $[OIII]5007/H\beta$ (the *BPT-NII diagram*). This diagram was studied in numerous work and the dividing lines have been developed and adapted as a function of the ionization models and/or observations available.

- **Star Forming Galaxies**:

$$\log(\frac{EW_{[NII]}}{EW_{H_{\alpha_{corr}}}}) > -0.4 \tag{1.14}$$

- **Transition Galaxies**:

$$-0.4 > \log(\frac{EW_{[NII]}}{EW_{H_{\alpha_{corr}}}}) > -0.22 \tag{1.15}$$

- **Strong AGN**:

$$\log(\frac{EW_{[NII]}}{EW_{H_{\alpha_{corr}}}}) > -0.4 \; and \; \log(\frac{EW_{[OIII]}}{EW_{H_{\beta}}}) > 0.5 \tag{1.16}$$

- **Weak AGN**:

$$\log(\frac{EW_{[NII]}}{EW_{H_{\alpha_{corr}}}}) > -0.4 \; and \; \log(\frac{EW_{[OIII]}}{EW_{H_{\beta}}}) < 0.5 \tag{1.17}$$

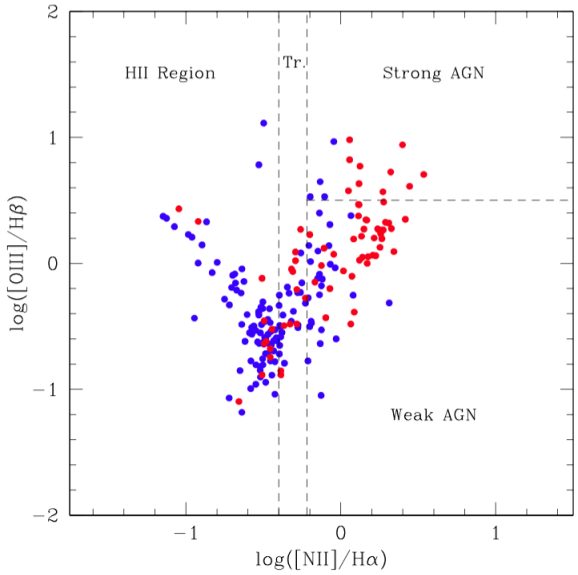

Figure 1.25: Example of BPT diagram. Different colors indicate galaxies whose spectra has been taken from different sources: blue for SDSS and red for NED.

1.6 Extrapolation of the Star Formation in the Nucleus to the Whole Galaxy

The principal sources of galaxy's spectra, SDSS and NED, provide the spectra of the nucleus, which has not necessarily the same form the whole galaxy's one. In the *Brinchmann et al (2004)* it is developed a method to make this correction.

This is a technique for aperture correction which uses the resolved color information available for each galaxy in the SDSS. Using this empirically based aperture correction it is possible to make an estimation of how the nuclear Star Formation changes when moving to the outer region.

The aperture correction scheme focuses on the probability distribution P (SFR/L_i |color), i.e. the probability of the specific star formation rate for a given set of colors. It has been chosen to normalize to the i-band luminosity. This is the reddest band with uniformly small photometric uncertainties. However, it has been verified that the results do not depend significantly on the choice of photometric band.

In theory it would be necessary to construct probabilities for SFR/L_i using all the color information available. It turns out, however, that $(g-r\ )$ and $(r-i)$ contain all the useful information necessary for the purpose and adding other colors does not significantly

improve the results.

The result of this procedure is illustrated in the figure (1.21). This shows P(SFR/L_i |color) for a subset of the full 0.1(g - r), 0.1(r - i) grid. The color is indicated as $(g-r)/(r-i)$ in the top left-hand corner of each panel and increases to the right for $(g-r)$ and upwards for $(r-i)$. The number of galaxies in each bin is also indicated in each panel as well as the number of galaxies that have colors in this bin outside the fibre. The thick and thin bars on the x-axis show the average and median SFR/Li for that bin, respectively.

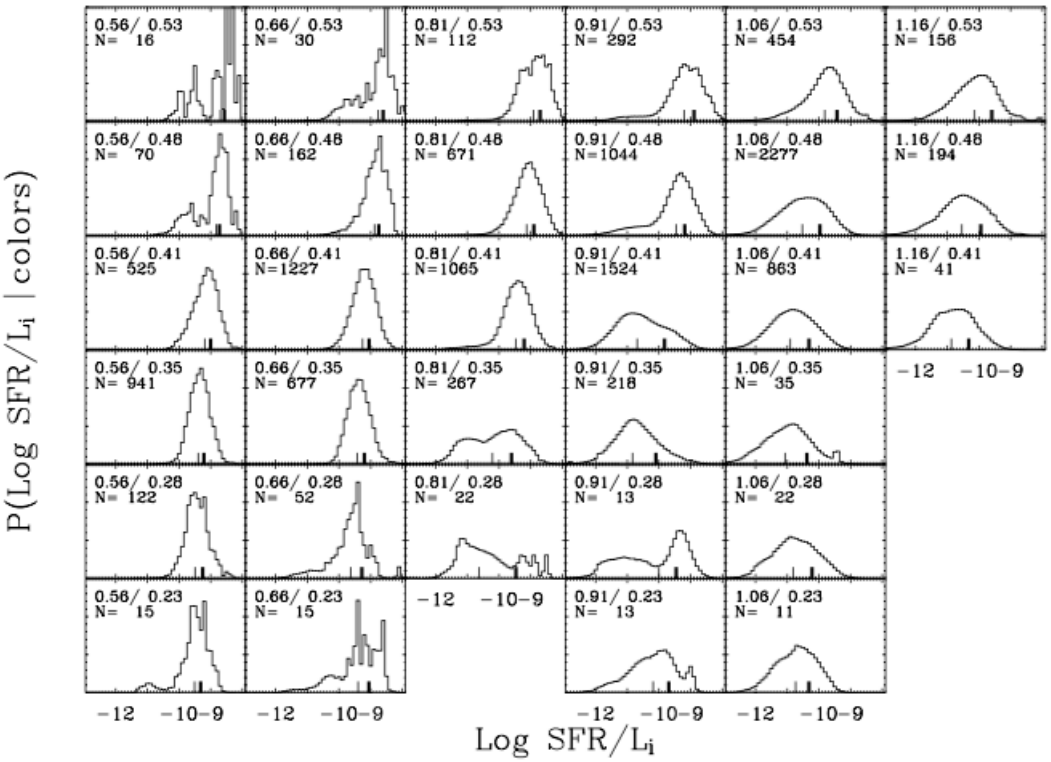

Figure 1.26: The probability distribution of log SFR/L_i in bins of $(g-r)$ and $(r-i)$. The $(g-r)$ color increases to the right and is indicated as the first number in the top left-hand corner of each panel. The second number gives the $(r-i)$ color and this increases upwards in the figure. The thick black mark on the x-axis shows the average SFR/L_i whereas the thin mark shows the median.

The shape of the distributions varies strongly with color and it is often not well represented by a Gaussian. In addition, higher values of SFR/Li often occur at redder (r - i) colors. This is because the emission lines around H contribute significantly to the i flux during an episode of star formation. The probability distribution also becomes very wide for galaxies with (gr) ≤ 0.7, $(r-i) \leq 0.5$ and their star formation rates are constrained to no better than a factor of 10. This region of color space is populated both by dusty

star-forming galaxies and by galaxies with old stellar populations.

It is important to emphasize that this method of aperture correction is purely empirical. The main assumption is that the distribution of SFR/L_i for given $(g-r)$, $(r-i)$ colors is similar inside and outside the fibre. Therefore, this assumption and the reliability of this procedure should clearly be tested.

Chapter 2

The Herschel Reference Sample

The Herschel Reference Sample (HRS) is a sample of 323 galaxies that has been studied in the *Herschel Reference Survey*. The goal of this survey has been to use the Herschel Space Observatory (built by the ESA, is one of the the largest infrared telescope ever launched) to improve our knowledge of the cold dust properties of the most common extragalactic sources populating the local universe. The measured data has allowed, for example, to trace for the first time the variation of the properties of the cold dust of normal galaxies along the Hubble sequence, study the role of dust in the physics of the Interstellar Medium, study the relationship between dust emission and star formation and determine the amount and origin of interstellar dust in ellipticals.

The criteria to choose this sample of galaxies have been the following:

- **Volume-limited:** A volume limit was imposed to reduce distance uncertainties due to local peculiar motions and ensure the presence of low-luminosity, dwarf galaxies, not accessible at high redshift. By applying a lower distance limit we exclude the very extended sources, the observing of which would be too time consuming.
- **K band selection:** Given the expected low dust content of quiescent galaxies, whose emission would be hardly detectable within reasonable integration times, a more stringent limit has been adopted for early-types than for star-forming galaxies.
- **High galactic latitude:** To minimize galactic cirrus contamination, galaxies have been selected at high galactic latitude and in low galactic extinction regions.

The resulting sample is composed of 323 galaxies located in the sky region with a R.A. between 10^h17^m and 14^h43^m and declination between -6^o and 60^o. The sample spans a large range in environment since it includes the Virgo cluster, many galaxy groups

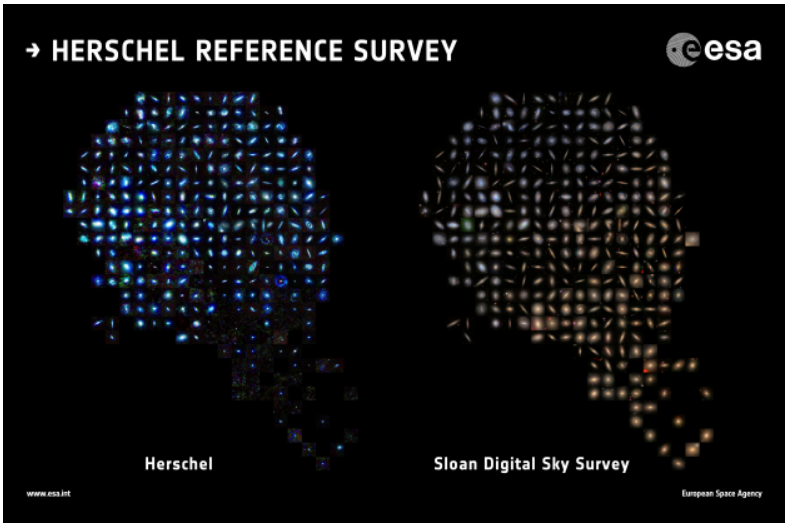

Figure 2.1: Collage of galaxies in the Herschel Reference Survey at infrared/submillimetre wavelengths by Herschel (left) and at visible wavelengths from the Sloan Digital Sky Survey (SDSS, right). The Herschel image is colored with blue representing cold dust and red representing warm dust; the SDSS image shows young stars in blue and old stars in red. Together, the observations plot young, dust-rich spiral/irregular galaxies in the top left, with giant dust-poor elliptical galaxies in the bottom right.

and pairs as well as relatively isolated objects (Figure 1.19). Using the Virgo cluster membership criteria defined in Gavazzi et al. (1999a), the HRS includes 82 members of cluster A and B. The other galaxies are members of nearby clouds such as Leo, Ursa Major and Ursa Major Southern Spur, Crater, Coma I, Canes Venatici Spur and Canes VenaticiCamelopardalis and Virgo-Libra Clouds.

As defined, the present sample is ideal for any statistical study of the mean galaxy population of the nearby universe.

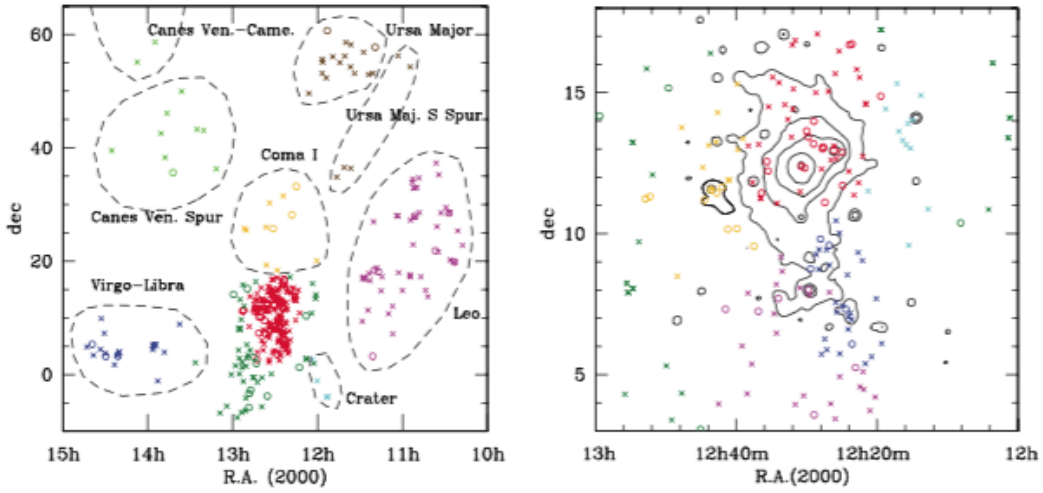

Figure 2.2: Sky distribution of the HRS (left panel). Dashed contours delimit the different clouds. The large concentration of galaxies in the center of the figure is the Virgo cluster (red) with its outskirts (dark green) Orange symbols are for Coma I Cloud, magenta for Leo Cloud, brown for Ursa Major Southern Spur and Cloud, cyan for Crater Cloud, light green for Canes Venatici Spur and Camelopardalis, and blue for Virgo-Lybra Cloud galaxies, respectively. The Virgo cluster region (right panel): black contours show the diffuse X-ray emission of the cluster . Red symbols are for galaxies belonging to the Virgo A cloud, blue to Virgo B, orange to Virgo E, magenta to Virgo S, cyan to Virgo N, and dark green to the Virgo outskirts, as defined by Gavazzi et al. (1999a).

Chapter 3

Data Sources

In order to analyze the spectra via the BPT diagram it is necessary to have the Equivalent Width of the lines $[NII]$, $[OIII]$, H_α and H_β. The data sources have been the following:

3.1 Nuclear Spectra

3.1.1 Observatory of Loiano

The observatory station in Loiano located in 1.2 km from the central station in a small town in the North Apennine ridge, about 37 km from Bologna and is a property of the University of Bologna is run by INAF (Astronomical Observatory of Bologna).
The observatory consists of two telescopes. A 60 cm telescope built by Zeiss and inaugurated in 1936 which is now used for outreach and teaching purposes, and a 152 cm primary mirror telescope (the second largest in Italy) inaugurated in 1976 which is dedicated to Giovanni Domenico Cassini, the famous italian mathematician astronomer and engineer who have built the sun dial of San Petronio in Bologna and the Paris observatory. The optical telescopes are installed and have been used by astronomers from both Bologna and abroad and the station is also a activity center.

The Telescope

Cassini telescope, with a diameter of 152 cm. Its system is very different from the classical one: there is a metal structure that holds the optics and it is not in a tube like in classical telescope.

Figure 3.1: Cassini Telescope

On the focal plane of the telescope there is an equipment in a box connected to the cell that holds the primary mirror; the equipment changes for different programs (photometers, spectrographs, CCD), but an ocular is always present that gives an optical field of 10', and a video acquisition system to check the pointing and the tracking.

The telescope is equipped with **BFOSC** (*Bologna Faint Object Spectrograph and Camera*). It is an instrument built around a stiff frame holding the collimator, the camera (the last optical element) and the detector to allow the acquisition of both images and spectra.

All images and spectra were reduced and analyzed using **IRAF** (*Image Reduction & Analysis Facility*). It is a collection of software written at the National Optical Astronomy Observatory (NOAO).

3.1.2 Sloan Digital Sky Survey

The Sloan Digital Sky Survey (SDSS) is a major multi-filter imaging and spectroscopic redshift survey using a dedicated 2.5-m wide-angle optical telescope at Apache Point Observatory in New Mexico, United States. The project was named after the Alfred P. Sloan Foundation, which contributed significant funding.
Data collection began in 2000, and the final imaging data release covers over 35% of the sky, with photometric observations of around 500 million objects and spectra for more than 3 million objects. The main galaxy sample has a median redshift of z = 0.1; there are redshifts for luminous red galaxies as far as z = 0.7, and for quasars as far as z = 5;

and the imaging survey has been involved in the detection of quasars beyond a redshift z = 6.

The survey makes the data releases available over the Internet. The SkyServer provides a range of interfaces to an underlying Microsoft SQL Server. Both spectra and images are available in this way, and interfaces are made very easy to use so that, for example, a full color image of any region of the sky covered by an SDSS data release can be obtained just by providing the coordinates. In most of the cases there are also available the measures of the EW of the emission lines. // In the cases that this data was not avaiable we used IRAF to get the emission lines from the downloaded spectra.

3.1.3 NASA/IPAC Extragalactic Database

The NASA/IPAC Extragalactic Database (NED) is an on-line astronomical database for astronomers that collates and cross-correlates astronomical information on extragalactic objects (galaxies, quasars, radio, x-ray and infrared sources, etc.).
NED was created in the late 1980s by two Pasadena astronomers, George Helou and Barry F. Madore. NED is funded by NASA and is operated by the Infrared Processing and Analysis Center (IPAC) on the campus of the California Institute of Technology, under contract with NASA.

NED is built around a master list of extragalactic objects for which cross-identifications of names have been established, accurate positions and redshifts entered to the extent possible, and some basic data collected. Bibliographic references relevant to individual objects have been compiled, and abstracts of extragalactic interest are kept on line. Detailed and referenced photometry, position, and redshift data, have been taken from large compilations and from the literature. It also includes images from 2MASS, from the literature, and from the Digitized Sky Survey.

NED contains 206 million distinct astronomical objects with 232 million cross-identifications across multiple wavelengths, with redshift measurements for 5 million objects, 1.9 billion photometric data points, 609 million diameter measurements, 71 thousand redshift-independent distances for over 15 thousand galaxies, 310 thousand detailed classifications for 230 thousand objects, and 2.6 million images, maps and external links, together with links to 65 thousand journal articles, notes and abstracts.

The EW of the emission lines have been taken from the *L. C. Ho; A. V. Filippenko; W. L. W. Sargent (1997). "A Search for "Dwarf" Seyfert Nuclei. III. Spectroscopic Parameters and Properties of the Host Galaxies". Astrophysical Journal Supplement 112: 315 390.*

Most of the nuclear spectra have been taken from SDSS (162) and NED (113), but

for some galaxies (47) there was not available data. In this cases the Observatory of Loiano has been used to get the spectra, although if it gets a more reduced region of the spectrum and doesn't allow to measure the EW of $[OIII]$ and $[H_\beta]$.

3.2 Spectra of the Whole Galaxy

The data was taken from *Boselli A. et al. (2013)*. In this paper Boselli shows the results obtained in a long-slit integrated spectroscopy of 238 late-type galaxies belonging to the Herschel Reference Survey.

For 233 galaxies it has been possible to measure the equivalent width of the $[NII]$ and $[H_\alpha]$ emission lines and are, therefore, valid for theclassification via WHAN diagram. The four emission lines required for the BPT diagram ($[NII]$, $[OIII]$, H_α and H_β), instead, have been measured for 168 out of 238 galaxies.

Chapter 4

Results

The following table collects the measured emission lines and the corresponding classification of each galaxy.

HRS	Nuclear							Whole Galaxy					
	Source	H_β	$[OIII]$	H_α	$[NII]$	BPT Clas.	WHAN Clas.	BPT Clas.	WHAN Clas.	H_β	$[OIII]$	H_α	$[NII]$
001	SDSS	3.533348	1.195192	8.958126	3.138068	H	H	H	H	3.11	1.19	22.12	6.650
002	LOIANO	...	...	33.43	11.39	...	H	H	H	5.66	2.85	36.76	11.310
003	NED	1.525	3.387	3.39	4.915	WA	WA	...	...	...	...	...	...
004	NED	5.539	32.73	16.29	21.67	SA	SA	H	H	4.00	7.00	34.80	0.000
005	SDSS	4.910075	0.9903799	12.17839	4.49391	H	H	...	...	0.0	9.03	3.040	...
006	SDSS	3.283762	1.417097	7.040781	2.061498	H	H	...	...	...	...	...	...
007	NED	0.8904	0.561	4.24	3.604	WA	WA	...	...	...	...	...	...
008	NED	0.2576	2.465	1.61	1.835	SA	RG	...	...	...	...	...	...
009	LOIANO	...	...	2.881	2.914	...	RG	...	...	...	...	...	...
010	SDSS	7.240343	1.980301	20.722	5.518867	H	H	H	H	6.11	6.04	33.64	8.050
011	SDSS	8.008218	1.90387	27.03592	7.848429	H	H	H	H	4.90	3.04	30.78	8.380
012	SDSS	7.723209	6.517807	29.19285	4.310708	H	H	H	H	7.02	9.13	37.57	6.530
013	SDSS	2.742141	2.829689	7.55966	4.822526	WA	SA	H	H	3.09	1.46	24.69	8.160
014	NED	0.8784	0.2899	2.44	2.83	WA	RG	...	...	...	...	...	...
015	NED	0.4851	0.4172	1.47	0.7203	T	RG	...	...	...	...	...	...
016	NED	4.876	1.121	28.68	9.178	H	H	H	H	2.78	1.27	18.08	5.750
017	NED	1.488	0.3571	6.2	2.046	H	H	H	H	7.06	6.16	36.44	9.690
018	SDSS	3.170857	10.71567	7.725147	4.899063	SA	SA	T	H	1.75	2.61	13.77	5.640
019	SDSS	55.51836	8.678452	255.1519	72.33173	H	H	H	H	6.58	2.52	37.39	11.560
020	NED	8.556	6.503	28.52	8.841	H	H	H	H	12.65	18.71	66.70	14.470
021	SDSS	4.331649	1.416637	8.628691	2.654546	H	H	H	H	1.54	1.38	14.52	3.410
022	NED	0.7564	1.664	2.44	3.587	WA	RG	...	...	...	...	...	...
023	LOIANO	...	...	20.834	13.82	...	SA	T	H	1.40	1.76	15.88	6.980
024	NED	3.839	0.8062	17.45	6.108	H	H	H	H	3.35	1.22	22.56	8.100
025	SDSS	18.00077	1.643904	70.40385	26.43243	H	H	H	H	6.00	3.71	38.21	12.680
026	SDSS	6.645896	5.338396	20.54405	4.121306	H	H	H	H	4.56	5.13	28.21	5.860
027	SDSS	7.85226	2.700128	26.80031	8.616503	H	H	H	H	10.12	6.42	50.40	15.990
028	LOIANO	...	...	8.72	3.08	...	H	H	H	7.88	3.06	32.46	8.540
029	SDSS	3.59579	1.396914	9.954664	2.943911	H	H	H	H	6.22	4.76	27.65	6.330
030	SDSS	4.432011	1.2508	8.99238	3.747602	T	H	H	H	5.64	4.13	34.52	8.720
031	NED	79.52	171	274.2	32.9	H	H	H	H	10.09	22.17	56.44	7.560
032	LOIANO	...	...	2.58	0.85	...	RG	...	...	...	...	...	...
033	LOIANO	...	...	9.1	3.92	...	H	H	H	3.49	1.50	19.96	7.030
034	SDSS	2.105493	0.6822028	4.278676	2.2641	T	WA	...	H	...	...	13.28	4.100
035	SDSS	0.2042666	0.4882029	0.5536794	0.6441507	WA	RG	...	RG	...	...	1.80	0.600
036	NED	14.07	7.455	61.16	36.08	T	SA	T	SA	5.68	2.79	30.30	17.760
037	SDSS	1.497563	3.043104	3.043104	2.585614	WA	WA	T	H	3.8	1.60	21.09	9.020
038	LOIANO	...	...	14.3	4.00	...	H	H	H	3.93	6.89	27.08	4.110
039	SDSS	3.692585	0.8351344	7.108813	2.528923	H	H	H	H	3.31	2.92	21.84	5.500
040	LOIANO	...	...	56.92	15.43	...	H	H	H	8.07	8.99	44.46	10.580
041	SDSS	4.743143	1.47025	14.21141	4.191411	H	H	...	...	...	...	...	...
042	NED	3.4047	5.2962	12.61	0.8827	H	H	...	H	3.59	...	21.09	7.660
043	NED	0.1056	0.3105	0.32	0.416	WA	RG	...	...	...	...	...	...

HRS	Nuclear							Whole Galaxy					
	Source	H_β	$[OIII]$	H_α	$[NII]$	BPT Clas.	WHAN Clas.	BPT Clas.	WHAN Clas.	H_β	$[OIII]$	H_α	$[NII]$
044	SDSS	104.3891	216.6493	530.6762	57.8698	H	H	H	H	20.64	43.26	104.90	14.470
045	LOIANO	...	...	1.3	1.5	...	RG	...	...	...	...	...	...
046	NED	0.5943	0.6834	2.83	4.754	WA	RG	...	...	...	...	...	...
047	SDSS	1.620251	0.9394188	1.674516	0.7761074	T	RG	H	H	3.59	5.30	25.90	5.370
048	NED	0.807	0.2582	2.69	1.157	T	RG	H	H	4.35	2.00	30.14	10.070
049	NED	...	...	...	...	Passive		...	...	...	...	...	...
050	SDSS	3.860193	5.347445	11.703	7.282123	WA	SA	H	H	4.24	1.33	30.78	10.630
051	SDSS	11.00273	4.209245	46.17787	13.73653	H	H	H	H	5.11	8.69	29.04	5.050
052	LOIANO	...	...	4.93	2.34	...	H	H	H	1.23	3.50	9.24	3.260
053	SDSS	2.724149	0.8737352	6.660133	2.683802	T	H	H	H	2.94	1.24	21.54	6.780
054	SDSS	1.224233	0.9176794	1.735304	1.316444	WA	RG	...	...	...	...	...	...
055	SDSS	2.992689	0.7533485	8.877333	2.904266	H	H	H	H	3.40	1.36	24.14	8.470
056	SDSS	2.755173	0.6151056	8.203703	3.306834	T	H	H	H	5.69	2.47	34.36	12.600
057	NED	17.27	2.245	59.54	18.46	H	H	H	H	3.53	0.0	20.60	7.160
058	LOIANO	...	...	5.244	2.047	...	H	...	H	-4.38	4.27	22.51	5.66
059	SDSS	1.774973	1.637441	3.110407	2.860091	WA	WA	H	H	1.86	1.45	12.93	4.800
060	NED	14.58	15.31	76.74	39.14	T	SA	T	H	1.20	1.65	11.92	5.770
061	SDSS	5.903831	3.613571	11.95847	2.541627	H	H	H	H	7.45	15.16	39.41	4.690
062	SDSS	3.45784	1.3433	8.031241	3.398049	T	H	H	H	5.00	41.85	84.36	8.500
063	SDSS	2.05915	0.6480523	3.874089	1.584609	T	H	...	H	...	...	11.82	4.120
064	SDSS	3.298012	0.5465748	4.727248	1.775982	H	H	H	H	2.50	1.80	14.20	2.600
065	LOIANO	...	...	11.97	2.70	...	H	H	H	6.16	10.95	31.92	4.870
066	NED	1.548	0.4644	8.6	3.096	H	H	H	H	4.74	3.54	35.02	10.120
067	SDSS	5.923004	4.137173	17.75432	3.711323	H	H	H	H	9.74	16.90	47.36	6.850
068	LOIANO	...	...	42.73	14.77	...	H	H	H	13.20	40.71	84.13	9.080
069	NED	...	...	1.821	1.425	...	RG	...	H	...	...	3.15	1.280
070	NED	...	...	16.92	3.21	...	H	H	H	13.87	16.55	47.11	6.840
071	NED	1.548	0.4644	8.6	3.096	H	H	...	...	...	...	...	...
072	NED	...	...	41.34	3.929	...	H	H	H	13.48	2.89	24.53	6.790
073	NED	0.3885	0.6061	1.85	2.238	WA	RG	H	H	2.72	0.14	9.16	3.520
074	SDSS	6.23049	57.7682	17.98286	16.20822	SA	SA	H	H	6.17	4.46	37.27	13.340
075	SDSS	5.034438	0.6523423	5.100862	1.831812	H	H	...	H	...	...	10.28	2.39
076	SDSS	23.38864	45.75806	95.18204	8.023966	H	H	H	H	7.86	19.91	39.99	4.500
077	LOIANO	...	...	1.98	1.36	...	RG	...	H	2.54	...	19.93	6.53
078	SDSS	3.564081	2.558907	7.492049	1.77536	H	H	H	H	4.23	5.81	23.92	4.320
079	SDSS	20.13481	34.10229	76.94807	7.972804	H	H	H	H	12.84	28.08	71.96	8.990
080	SDSS	15.46932	5.538929	63.3802	21.41545	H	H	H	H	2.44	0.0	18.26	5.620
081	SDSS	4.379025	2.90506	14.97091	11.22067	WA	SA	...	H	...	...	14.30	6.600
082	SDSS	14.32356	3.441399	50.56691	12.1844	H	H	...	...	...	...	...	...
083	SDSS	32.34327	45.2705	125.0064	15.886	H	H	H	H	6.68	12.30	38.34	5.910
084	LOIANO	...	...	1.3	1.866	...	RG	T	H	1.39	0.0	12.46	5.020
085	NED	7.682	1.383	40.43	14.15	H	H	T	H	3.28	1.66	15.18	6.390
086	SDSS	2.962531	0.8712546	10.2269	3.141417	H	H	H	H	10.71	4.45	37.87	8.390
087	SDSS	1.988657	0.3338847	4.7104	1.656639	H	H	...	...	...	...	...	...
088	SDSS	...	...	140.3098	65.0287	...	H	T	H	3.80	1.49	21.65	9.500
089	NED	5.539	1.939	17.31	5.539	H	H	H	H	5.27	8.41	32.89	6.000
090	NED	...	...	...	...	Passive		...	...	...	...	...	...
091	NED	0.3248	0.6074	4.64	6.542	WA	WA	H	H	1.03	0.46	9.06	3.560
092	SDSS	4.012769	0.9765098	9.037971	3.335566	H	H	H	H	3.74	1.81	19.31	5.630
093	NED	1.523	2.391	1.57	2.889	WA	RG	...	...	...	...	...	...
094	SDSS	1.47771	0.8653391	2.316607	1.218154	T	RG	H	H	5.13	3.85	18.90	4.590
095	SDSS	5.742653	1.48529	18.18419	5.871779	H	H	H	H	2.45	1.18	19.00	5.170
096	NED	9.681	1.355	46.1	18.9	T	H	...	H	2.97	...	19.66	6.540
097	NED	0.1978	0.4134	0.86	1.754	WA	RG	...	H	...	...	4.97	1.430
098	LOIANO	...	...	18.48	5.113	...	H	H	H	3.08	3.18	23.69	5.400
099	SDSS	...	...	4.168	1.707	...	H	H	H	4.04	1.45	21.36	5.570
100	SDSS	1.558097	0.5418495	3.214049	1.539352	T	H	...	H	...	...	12.14	3.150
101	NED	...	...	...	...	Passive		...	...	...	...	...	...
102	NED	1.29	1.161	8.06	3.869	T	H	H	H	4.86	1.18	31.49	10.20
103	SDSS	1.706486	0.8282546	1.215927	2.496723	WA	RG	...	RG	...	...	2.95	1.230
104	SDSS	7.578852	2.128129	17.79574	4.585313	H	H	...	H	...	...	18.48	4.280
105	NED	...	...	...	...	Passive		Passive		...	...	...	...
106	SDSS	2.93733	0.6687233	8.040657	2.565623	H	H	...	H	...	...	18.48	4.280
108	LOIANO	...	...	22.75	6.748	...	H	...	H	2.50	...	18.03	5.570
109	SDSS	2.277025	1.33827	4.326168	2.373547	T	WA	...	H	...	2.28	11.03	3.620
110	SDSS	17.32181	17.40827	86.09368	10.32445	H	H	H	H	12.51	16.3	51.16	7.700
111	SDSS	13.99368	2.189672	47.42817	14.90869	H	H	...	H	...	...	14.04	4.300
112	SDSS	2.03603	1.083576	5.240491	3.22701	WA	WA	...	H	...	...	3.15	1.290
113	SDSS	5.089184	0.0	4.208219	4.198048	WA	WA	...	...	...	...	...	...
114	NED	3.08	4.066	12.32	9.61	WA	SA	T	H	5.36	1.69	31.40	12.560
115	SDSS	5.759659	3.223043	22.28787	8.938683	T	H	...	H	...	...	5.15	1.970
116	SDSS	0.1054069	0.3189989	0.0	0.1198477	...	RG	...	...	...	...	...	...
117	SDSS	2.282863	0.0	4.969091	2.188175	T	H	...	...	...	...	...	...
118	LOIANO	...	...	18.3	3.608	...	H	H	H	11.56	31.34	55.52	6.080
119	SDSS	2.222946	13.4556	16.83322	4.977768	H	H	...	H	...	...	7.37	2.250
120	SDSS	0.3380514	1.144752	1.988661	1.562198	SA	RG	...	...	...	...	...	...
121	SDSS	2.284674	0.706879	5.109979	2.700316	T	WA	...	H	...	...	12.22	3.750
122	NED	1.727	1.364	7.85	9.263	WA	SA	...	H	3.05	...	20.00	7.210

HRS	Nuclear							Whole Galaxy					
	Source	H_β	$[OIII]$	H_α	$[NII]$	BPT Clas.	WHAN Clas.	BPT Clas.	WHAN Clas.	H_β	$[OIII]$	H_α	$[NII]$
122	NED	1.727	1.364	7.85	9.263	WA	SA	...	H	3.05	...	20.00	7.210
123	NED	0.5934	1.003	0.69	0.4347	WA	RG	...	...	...	...	...	...
124	LOIANO	...	...	6.11	0.00	...	H	...	H	...	0.64	9.37	2.070
125	NED	...	...	...	...	Passive		...	...	...	...	...	...
126	NED	...	...	...	...	Passive		...	...	...	...	...	...
127	SDSS	1.200018	0.9146786	3.032504	2.151407	WA	WA	...	H	...	...	6.20	1.810
128	SDSS	7.706888	2.38603	22.78905	6.062415	H	H	...	H	3.07	...	16.75	2.590
129	NED	0.2016	0.3306	0.63	0.8568	WA	RG	...	...	...	...	...	...
130	SDSS	22.25593	7.291203	83.19791	19.09277	H	H	H	H	4.73	2.45	26.81	6.990
131	SDSS	5.34689	1.390786	10.73412	4.389906	T	SA	...	...	...	...	...	...
132	LOIANO	...	...	42.33	4.726	...	H	H	H	13.00	18.1	48.15	10.04
133	SDSS	2.979615	1.731909	9.27983	2.106915	H	H	H	H	2.43	4.11	20.76	4.050
134	LOIANO	...	...	...	...	...	...	...	H	...	...	7.78	3.400
135	NED	...	...	...	...	Passive		Passive		...	...	...	...
136	SDSS	0.7635874	0.5360605	1.41763	1.508873	...	RG	...	...	...	...	...	...
137	NED	...	...	...	...	Passive		Passive		...	...	...	...
138	NED	0.4368	0.7513	2.08	3.765	WA	RG	...	...	...	...	...	...
139	LOIANO	...	...	30.04	5.168	...	H	H	H	14.12	14.70	46.17	9.650
140	NED	0.2408	0.9849	0.86	2.391	SA	RG	...	...	...	...	...	...
141	SDSS	0.9294148	0.7626585	2.02318	1.473164	WA	RG	...	H	...	...	6.77	2.370
143	SDSS	5.111989	1.330408	6.340428	2.545194	T	H	H	H	8.65	17.40	45.09	8.460
144	SDSS	65.8823	636.1177	237.3147	133.3445	T	SA	T	H	7.09	37.46	36.50	15.640
145	SDSS	1.429016	0.4792456	0.8378344	0.5413775	WA	RG	H	H	4.15	4.63	26.65	5.650
146	SDSS	18.13267	7.54038	54.41082	11.88855	...	H	H	H	3.00	2.73	22.22	5.050
147	SDSS	4.075238	0.9394294	1.980621	1.458309	WA	RG	...	H	...	...	8.12	2.570
148	LOIANO	...	...	63.62	13.34	...	H	H	H	5.75	6.74	35.05	6.560
149	SDSS	3.39046	0.8055146	10.39418	3.299068	H	H	...	H	0.93	...	11.94	3.750
150	NED	...	...	...	...	Passive		Passive		...	...	...	...
151	SDSS	9.452365	1.650656	31.7796	9.937462	H	H	...	H	2.25	...	19.01	5.970
152	SDSS	14.82606	37.20267	61.01436	44.36751	WA	SA	T	H	4.06	1.48	26.34	10.660
153	SDSS	...	...	58.5544	44.2873	...	SA	H	H	3.45	0.85	22.83	7.050
154	SDSS	...	...	4.0221	1.4638	...	H	H	H	3.17	1.60	18.88	4.550
155	NED	...	...	...	...	Passive		Passive					
156	LOIANO	...	...	4.775	5.551	...	WA	...	WA	...	...	4.49	2.780
157	SDSS	4.509269	1.293274	9.978889	3.514616	H	H	H	H	7.25	5.31	40.58	10.440
158	SDSS	29.7607	70.33579	118.2627	8.433229	H	H	H	H	6.03	12.81	31.81	3.330
159	SDSS	16.03389	2.263542	72.15845	21.76218	H	H	...	SA	3.24	...	17.03	11.120
160	SDSS	3.489288	45.28904	10.2529	3.257454	H	H	...	H	2.11	...	16.96	6.580
161	NED	0.2992	0.3172	1.76	2.323	WA	RG	...	...	...	...	...	...
162	NED	0.5088	0.3612	3.18	2.162	WA	WA	...	...	...	...	...	...
163	NED	1.921	3.054	11.3	18.53	WA	SA	...	WA	...	...	4.63	4.560
164	LOIANO	...	...	2.78	0.23	...	H	...	...	...	...	...	...
165	SDSS	8.19343	2.401416	21.42179	6.062085	H	H	H	H	4.28	4.61	29.74	6.120
166	NED	...	...	...	...	Passive				Passive			
...	...	...	...										
167	SDSS	4.571216	1.58761	9.37178	6.026564	WA	SA	...	H	...	...	5.11	1.880
168	SDSS	8.372225	13.5026	33.07656	3.620806	H	H	H	H	9.85	24.94	48.99	4.990
169	SDSS	2.332953	0.7339891	3.988883	2.512889	WA	WA	H	H	0.61	2.23	7.57	1.160
170	NED	1.127	2.389	2.89	5.607	WA	RG	...	H	...	...	3.65	1.700
171	...	...	...	...	...	...	...	H	H	3.41	0.76	21.81	6.530
172	SDSS	2.823351	0.7714031	9.102161	3.086924	H	H	...	H	...	...	8.36	2.490
173	NED	1.17	1.018	4.5	4.68	WA	WA	...	WA	...	...	5.89	3.670
174	NED	0.4402	0.1805	1.42	1.732	WA	RG	...	...	...	...	...	...
175	NED	...	...	...	...	Passive		Passive		...	...	...	...
176	SDSS	0.4012482	0.4851913	4.316402	2.381514	T	WA	...	...	...	...	...	...
177	SDSS	9.637493	3.062775	29.11511	7.988356	H	H	H	H	6.45	3.71	31.12	7.710
178	NED	0.0363	0.1844	0.11	0.3773	SA	RG	...	...	...	...	...	...
179	NED	...	...	...	...	Passive		Passive					
180	NED	0.728	2.694	2.8	5.236	SA	RG	...	...	...	...	...	...
181	NED	...	...	...	...	Passive		...	...	...	...	...	...
182	SDSS	2.849561	0.4780665	2.011544	1.233619	WA	RG	H	H	8.25	2.25	24.21	5.490
183	NED	3.574	6.755	15.54	32.94	WA	SA	...	...	...	...	...	...
184	SDSS	11.25797	0.9607781	39.72654	7.556823	H	H	...	...	...	...	8.19	...
185	LOIANO	...	...	...	...	...	...	...	...	0.85	...	...	...
186	NED	0.1344	0.1559	0.24	0.3864	WA	RG	...	...	...	...	...	...
187	NED	263.995	520.855	713.50	85.62	H	H	H	H	6.59	3.76	32.22	8.350
188	LOIANO	...	...	15.05	4.854	...	H	H	H	5.98	1.96	25.53	6.590
189	LOIANO	...	...	18.92	4.416	...	H	H	H	6.96	2.33	38.66	9.790
190	NED	1.117	5.932	3.99	8.379	SA	WA	...	H	0.76	...	9.40	3.550
191	SDSS	2.803529	1.22672	3.997116	1.25238	H	H	H	H	6.13	6.98	24.33	4.600
192	SDSS	2.379345	0.3995789	7.531775	1.979206	H	H	...	H	...	...	5.55	1.060
193	SDSS	...	...	53.17	10.88	...	H	H	H	12.63	5.83	57.24	13.360
194	NED	0.7332	0.9018	5.64	2.876	T	WA	H	H	2.84	2.92	15.94	3.560
195	SDSS	0.2559804	0.3578313	0.0	0.150212	...	RG	...	...	...	...	...	...
196	SDSS	15.95095	3.697093	55.28689	16.42819	H	H	H	H	4.76	6.54	31.95	6.740
197	SDSS	11.62	1.75712	43.98034	13.27023	H	H	H	H	2.01	1.37	18.84	6.290
198	SDSS	1.323347	0.5506214	2.44496	1.208131	T	RG	H	H	2.16	1.93	13.95	3.070
199	SDSS	11.05874	1.555151	43.99196	9.83863	H	H	H	H	5.35	1.62	34.31	9.720

HRS	Nuclear							Whole Galaxy					
	Source	H_β	$[OIII]$	H_α	$[NII]$	BPT Clas.	WHAN Clas.	BPT Clas.	WHAN Clas.	H_β	$[OIII]$	H_α	$[NII]$
200	NED	0.3852	0.1425	2.14	1.712	WA	RG	WA	...	...	...	...	...
201	NED	0.602	0.5779	6.02	4.515	WA	WA	...	H	1.48	...	14.59	5.990
202	SDSS	0.3283044	0.09327056	0.0	0.0	...	RG	...	...	...	...	...	...
203	NED	108.3	293.5	433.1	38.98	H	H	H	H	17.43	38.11	98.97	11.490
204	NED	11.9	1.547	54.1	22.18	T	H	...	H	1.61	...	13.42	5.070
205	NED	5.842	1.928	30.75	14.45	T	H	H	H	3.08	2.65	26.22	9.780
206	LOIANO	...	...	4.201	1.442	...	H	H	H	7.29	0.68	41.15	11.970
207	LOIANO	...	...	6.469	3.005	...	H	...	H	1.36	...	13.43	4.150
208	NED	0.836	0.9363	2.09	2.884	WA	RG	...	H	...	...	4.87	1.690
209	NED	...	...	...	...		Retired	...	...	...	...	...	...
210	NED	0.534	0.9932	1.78	0.979	T	RG	...	...	...	...	...	...
211	NED	0.228	0.2576	0.76	1.14	WA	RG	...	...	...	...	...	...
212	SDSS	6.971085	14.8786	27.84477	3.784922	H	H	H	H	9.47	22.32	40.50	4.520
213	NED	0.288	2.514	1.44	3.6	SA	RG	...	...	...	...	...	...
214	NED	...	...	...	...		Passive	...	...	...	...	...	...
215	SDSS	2.313953	0.2890043	9.825578	2.97472	H	H	H	H	1.44	0.02	16.27	4.760
216	SDSS	3.347078	0.8590728	15.45823	5.92635	H	H	H	H	2.53	0.37	21.26	6.830
217	NED	0.288	2.514	1.44	3.6	SA	RG	...	WA	...	...	4.81	2.750
218	NED	...	...	...	...		Passive	...	...	...	...	...	...
219	NED	...	...	...	...		Passive	...	...	...	...	...	...
220	NED	2.269	6.966	7.32	13.83	WA	SA	...	WA	...	...	4.88	3.520
221	SDSS	2.381094	1.329581	5.655554	6.794061	WA	WA	...	H	...	...	8.26	2.710
222	SDSS	6.106132	0.6695638	23.10594	6.530777	H	H	...	H	...	...	7.32	2.320
223	SDSS	9.948657	4.645325	32.94497	6.287755	H	H	H	H	5.05	7.70	31.46	2.340
224	SDSS	1.016505	4.518838	5.69973	4.193941	SA	WA	...	WA	...	...	3.28	2.180
225	LOIANO	...	...	9.668	0.00	...	H	H	H	1.48	3.02	23.00	8.650
226	SDSS	6.439883	1.481309	20.81841	7.160069	H	H	...	...	...	...	...	...
227	SDSS	5.952156	3.092298	14.17525	2.517552	H	H	H	H	7.94	13.24	45.48	7.000
229	SDSS	...	...	...	...		Passive	...	...	...	...	...	...
230	LOIANO	...	...	14.19	3.849	...	H	H	H	2.97	2.14	20.24	5.490
231	NED	0.3102	0.3102	0.66	0.9768	WA	RG	WA	...	...	...	...	...
232	LOIANO	...	...	18.76	5.622	...	H	...	H	...	...	5.85	2.060
233	SDSS	5.596941	3.916048	15.03695	8.427251	T	SA	...	H	1.04	...	11.57	3.880
234	NED	...	...	...	...		Passive		Passive				
235	NED	...	...	...	...		Passive	...	...	...	...	...	...
236	NED	...	...	...	...		Passive		Passive				
237	LOIANO	...	...	247.1	66.57	...	H	H	H	7.91	1.47	44.79	12.400
238	SDSS	2.479717	0.910417	6.836315	0.7757381	H	H	H	H	2.15	4.56	14.63	1.870
239	LOIANO	...	...	30.08	12.82	...	H	H	H	2.32	1.26	19.41	7.190
240	NED	...	...	...	...		Passive		Passive				
241	NED	0.4935	0.908	1.41	2.651	WA	RG	WA	...	...	...	...	...
242	NED	0.496	1.87	1.6	1.792	SA	RG	T	H	0.98	1.30	10.22	4.200
243	NED	0.1998	0.2677	0.54	0.9666	WA	RG	...	...	...	...	...	...
244	NED	3.715	0.2972	14.29	3.144	H	H	...	H	4.11	...	29.77	8.310
245	NED	...	...	...	...		Passive		Passive	...	...	...	...
246	NED	0.6528	1.201	1.92	3.533	WA	RG	H	H	2.43	1.03	15.19	5.740
247	SDSS	10.43378	1.058118	40.04209	10.49586	H	H	H	H	8.00	3.33	37.86	10.440
248	NED	...	...	...	...		Passive		Passive	...	...	...	...
249	LOIANO	...	...	3.081	0.14	...	H	...	...	...	...	...	...
250	NED	...	...	...	...		Passive	...	...	...	...	...	...
251	NED	...	...	8.244	4.253	...	SA	...	...	...	...	...	...
252	SDSS	4.437801	3.658223	11.02104	2.281496	H	H	H	H	4.47	9.41	28.73	4.800
253	LOIANO	...	...	72.22	20.23	...	H	...	...	...	...	...	...
254	SDSS	0.9585484	0.4625328	2.434438	1.43804	T	RG	...	H	1.66	...	17.99	5.490
255	SDSS	...	...	4.394	1.338	...	H	...	...	...	...	...	...
256	SDSS	14.02405	6.119386	63.75933	22.09196	H	H	...	...	...	...	...	...
257	NED	0.7316	3.139	2.36	3.092	SA	RG	SA	...	...	...	...	1.350
258	...	...	...	...	...	...	...	...	...	...	...	...	...
259	LOIANO	...	...	21.84	5.117	...	H	H	H	6.70	6.87	44.04	10.60
260	NED	0.9633	0.5972	5.07	2.636	T	WA	...	...	...	...	...	...
261	SDSS	...	...	8.1968	2.2325	...	H	...	H	1.26	...	11.68	3.080
262	SDSS	2.319243	1.501648	5.413014	2.446884	T	H	H	H	11.17	12.65	59.40	11.77
263	NED	0.3441	2.285	1.11	1.265	SA	RG	...	...	...	...	...	...
264	NED	...	...	7.997	1.864	...	H	...	H	1.36	...	12.31	2.260
265	NED	...	...	31.92	2.939	...	H	H	H	10.02	20.49	54.1	7.470
266	LOIANO	...	...	25.35	4.704	...	H	H	H	7.56	6.67	44.12	9.830
267	LOIANO	...	...	14.12	3.663	...	H	H	H	10.91	17.70	68.5	13.91
268	LOIANO	...	...	30.18	12.47	...	H	H	H	7.35	8.49	43.26	13.84
269	NED	...	...	...	...		Passive		Passive	...	...	...	...
270	LOIANO	...	...	1.30	1.326	...	RG	...	...	...	...	...	...
271	LOIANO	...	...	13.3	4.154	...	H	H	H	3.50	2.90	18.10	2.800
272	NED	0.1507	0.1869	0.11	0.242	WA	RG	H	...	...	...	...	...
273	SDSS	1.171182	0.6588151	3.806209	2.772256	WA	WA	...	H	0.85	...	10.30	3.390
274	NED	0.6789	1.982	2.19	2.869	WA	RG		H	...	...	3.07	0.900
275	NED	...	...	17.65	3.638	...	H	H	H	11.00	14.00	46.1	9.526
276	SDSS	12.68754	1.440942	51.58604	16.89756	H	H	...	...	...	...	...	...
277	SDSS	1.357304	1.334392	2.628844	2.24903	WA	RG	...	H	...	...	7.51	2.790
278	SDSS	...	...	11.1096	2.1955	...	H	...	H	...	...	5.67	1.960

HRS	Nuclear						Whole Galaxy					
	Source	H_β	$[OIII]$	H_α	$[NII]$	BPT Clas.	WHAN Clas.	BPT Clas.	WHAN Clas.	H_β	$[OIII]$	H_α	$[NII]$
279	SDSS	4.967571	2.228593	15.74361	4.807565	H	H	..	...	...	...	...	...
280	SDSS	1.466639	2.026252	2.773662	2.326083	WA	RG	..	H	2.10	...	14.12	5.210
281	SDSS	6.924461	2.71177	31.79533	7.899062	H	H	H	H	3.41	2.32	23.82	6.290
282	LOIANO	...	...	...	...	Passive			...	...	...	...	...
283	SDSS	5.34558	1.028316	17.82726	6.047186	H	H	H	H	6.98	5.47	36.71	14.17
284	NED	...	...	22.5	4.1	...	H	H	H	3.18	1.83	26.10	9.390
285	SDSS	2.408852	3.017472	11.37287	8.089664	WA	SA	...	WA	...	...	3.64	3.450
286	NED	0.3978	0.7479	1.53	2.647	WA	RG	H	...	...	...	...	...
287	SDSS	28.28437	7.943557	104.4154	31.55824	H	H	H	H	3.89	2.74	25.05	7.470
288	NED	...	...	4.18	8.562	...	WA	...	SA	...	4.65	7.27	5.210
289	LOIANO	...	...	8.323	5.014	...	SA	...	H	1.70	...	13.65	5.320
290	SDSS	9.658431	3.98982	37.92168	11.165	H	H	H	H	3.05	2.62	22.27	6.700
291	LOIANO	...	...	2.52	0.51	...	RG	...	...	...	...	...	...
292	SDSS	3.843987	0.6196117	13.06484	5.654074	T	H	...	H	5.17	...	33.82	12.90
293	SDSS	...	...	5.9335	2.4006	...	H	H	H	13.51	14.29	69.15	14.42
294	SDSS	2.647593	1.224732	5.336049	2.132809	T	H	H	H	2.62	1.55	19.73	5.66
295	NED	1.098	0.3622	7.84	4.077	T	SA	H	H	6.00	1.00	22.67	8.34
296	SDSS	...	...	4.973	5.434	...	WA	...	...	...	...	...	...
297	SDSS	2.657466	0.789086	6.009255	2.259524	H	H	H	H	2.56	3.03	20.31	5.20
298	LOIANO	...	...	10.80	3.84	...	H	H	H	7.49	6.85	44.51	12.16
299	SDSS	6.185344	1.502947	17.99173	6.946484	H	H	H	H	2.29	1.33	14.83	4.28
300	SDSS	3.41314	1.011408	1.659054	1.242979	WA	RG	...	H	...	...	3.91	1.36
301	SDSS	6.775189	0.6055271	2.365178	1.763887	WA	RG	H	H	2.48	2.33	16.72	5.02
302	LOIANO	...	...	11.61	4.53	...	H	H	H	2.29	3.00	18.76	3.33
303	LOIANO	...	...	69.69	24.23	...	H	H	H	7.74	4.18	46.49	16.18
304	SDSS	...	...	6.1655	2.0795	...	H	..	H	...	...	9.28	2.89
305	SDSS	7.102529	0.4659237	24.00399	5.514603	H	H	H	H	2.38	0.75	17.94	5.19
306	NED	0.4512	1.074	3.76	4.888	WA	WA	...	...	...	...	...	...
307	SDSS	0.9965827	0.190135	3.119591	1.250448	T	WA	...	...	...	...	...	...
308	SDSS	6.833901	4.3925	19.88034	3.924979	H	H	H	H	0.63	1.14	7.39	1.450
309	SDSS	...	...	14.1688	2.9197	...	H	H	H	7.32	12.11	34.65	4.790
310	SDSS	...	...	13.0024	3.7572	...	H	H	H	2.88	1.28	19.25	6.660
311	NED	0.1377	0.2547	0.51	0.8925	WA	RG	...	...	...	...	...	...
312	NED	...	...	...	...	Passive		...	...	...	...	...	...
313	LOIANO	...	...	7.38	3.45	...	H	H	H	2.18	1.41	15.38	3.540
314	SDSS	11.65149	10.52432	42.40291	9.749278	H	H	H	H	7.24	14.27	43.04	7.610
315	SDSS	82.36397	187.5986	397.3163	29.79506	H	H	H	H	16.20	42.31	79.23	7.490
316	NED	...	...	...	...	Passive		...	...	...	...	...	...
317	SDSS	6.123983	3.024251	14.48632	4.54704	H	H	H	H	3.68	3.34	21.79	5.390
318	SDSS	16.40744	16.7133	67.00605	10.66158	H	H	H	H	5.14	7.34	29.70	5.200
319	SDSS	...	...	80.3306	17.06	...	H	H	H	4.73	6.68	32.84	7.270
320	SDSS	2.538738	0.6379905	0.5094738	0.475527	WA	RG	H	H	5.31	5.16	29.43	6.380
321	SDSS	6.966376	2.808871	23.30001	6.881231	H	H	H	H	6.67	5.41	37.23	9.770
322	NED	0.3772	0.5922	0.82	0.6232	WA	RG	...	...	...	...	...	...
323	SDSS	4.008322	0.7680349	13.0495	4.25734	H	H	H	H	1.79	1.05	17.48	5.260

In the case of passive galaxies we didn't measure the lines because there was not necessity of making any classification.

4.1 Comparison between the BPT and WHAN diagram

The aim of this section is to compare the results of this two ways of classifying a galaxy. The BPT and WHAN diagram for the nuclear spectra is shown in the figure (4.1).

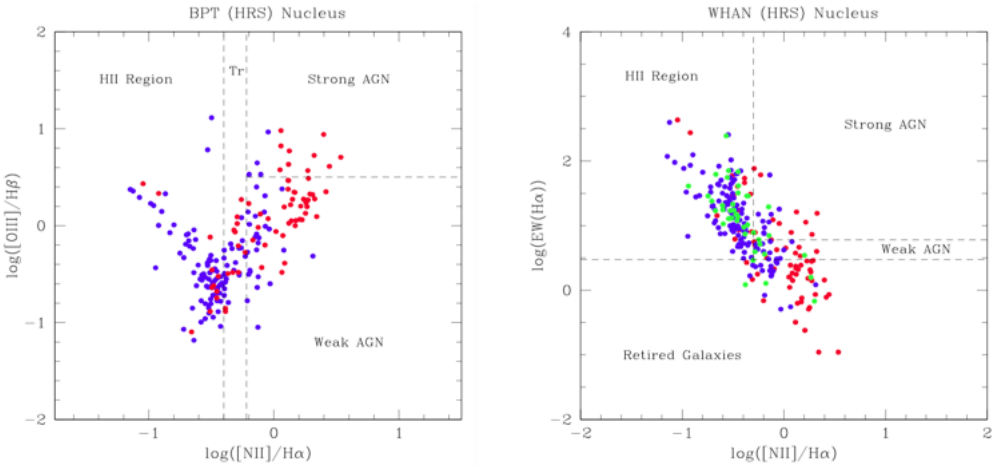

Figure 4.1: Left: BPT diagram containing all the nuclear spectra with the $[NII]$, $[OIII]$, H_α and H_β lines measured. Red dots indicate galaxies whose spectra has been taken from NED and blue from SDSS. Right: WHAN diagram containing all the nuclear spectra with the $[NII]$ and $H_\alpha$lines measured. Green dots indicate galaxies whose spectra has been taken from the Loiano Observatory.

A comparison between both classification methods is illustrated in the figures (4.2) and (4.3). On the one side we have the BPT diagram (or WHAN) and the colors of the dots are determined according to the BPT classification criteria. On the other side we have the WHAN (or BPT) diagram but the dots maintain the same color that was determined on the previous one. Therefore we are able to evaluate how do the different types of galaxies move when passing to the other kind of diagram.

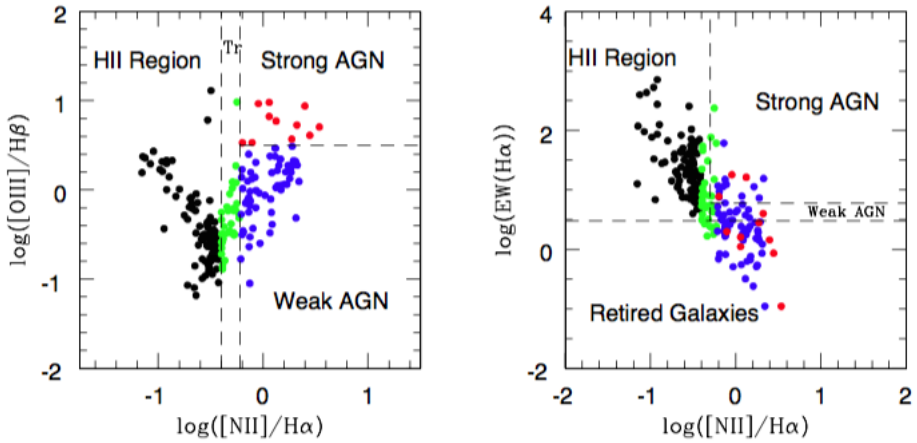

Figure 4.2: Illustration of how do the type of the galaxies change from BPT to WHAN diagram. The color of the dots is determined according to the diagram on the left and maintained on the right side. That is, the color of the dots in the WHAN diagram are fixed following the BPT diagram's criteria.

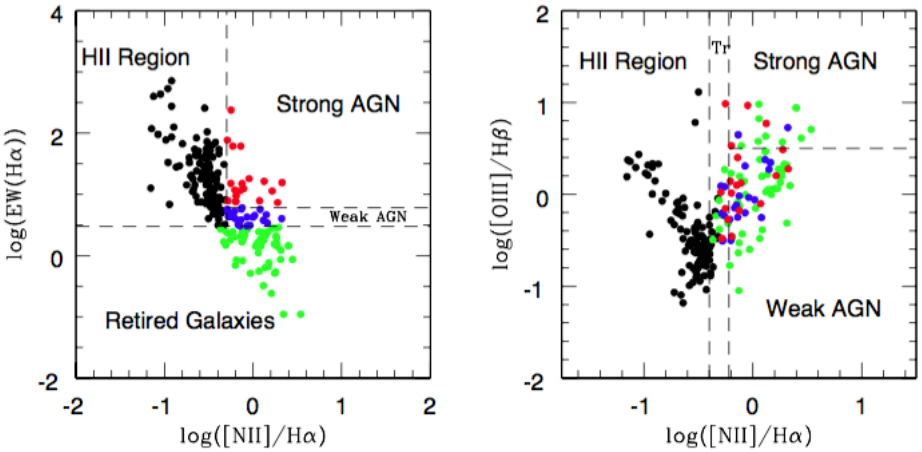

Figure 4.3: Illustration of how do the type of the galaxies change from WHAN to BPT diagram. The color of the dots is determined according to the diagram on the left and maintained on the right side. That is, the color of the dots in the BPT diagram are fixed following the WHAN diagram's criteria.

The following tables quantify these transitions. The first column shows the quantity of galaxies of each type determined by BPT (or WHAN, in the second table) and at the right we can see their classification obtained via the WHAN (or BPT) diagram.

BPT Clas.	**WHAN Clas.**			
	Strong AGN	*Weak AGN*	*Retired*	*HII Region*
Strong AGN (11) →	3 (27%)	1 (9%)	7 (64%)	0
Weak AGN (64) →	12 (19%)	15 (23%)	37 (58%)	0
Transition (35) →	5 (14%)	6 (17%)	6 (17%)	18 (52%)
HII Region (96) →	0	0	0	96 (100%)

WHAN Clas.	**BPT Clas.**			
	Strong AGN	*Weak AGN*	*Transition*	*HII Region*
Strong AGN (19) →	3 (16%)	11 (58%)	5 (26%)	0
Weak AGN (26) →	2 (8%)	18 (69%)	6 (23%)	0
Retired (47) →	9 (19%)	6 (13%)	32 (68%)	0
HII Region (114) →	0	0	12 (10.5%)	102 (89.5%)

These results are illustrated graphically in figures (4.4) and (4.5).

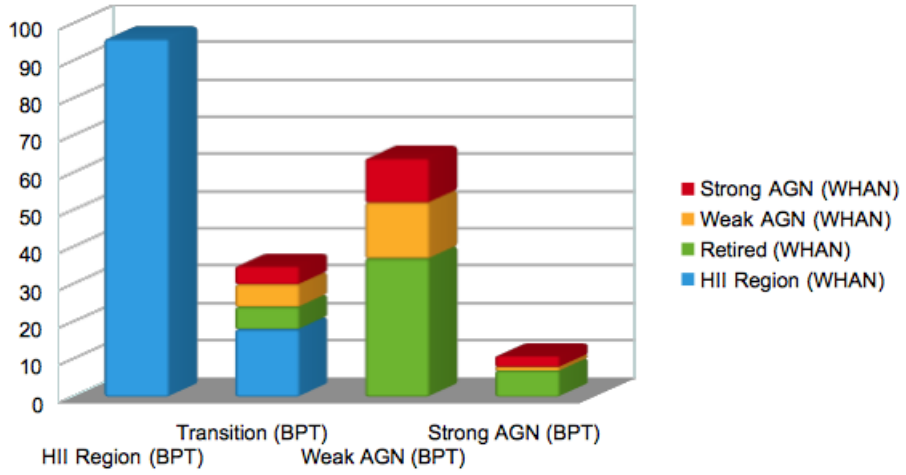

Figure 4.4: The BPT classification of the galaxies whose type has also been determined via WHAN diagram. For instance, in the first column we can see that all the galaxies determined *HII Region* are blue and, therefore, are also star forming regions under the WHAN's criteria. We can also comprobe that on the following columns both classification method diverge and don't predict the same types.

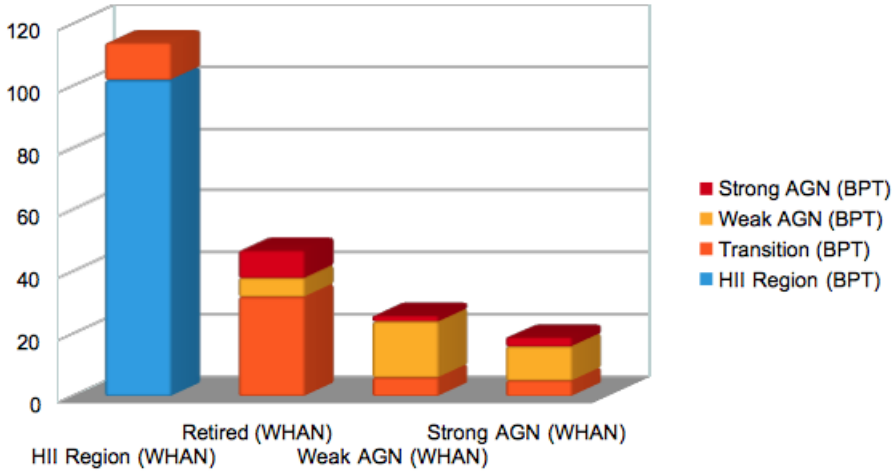

Figure 4.5: The WHAN classification of the galaxies whose type has also been determined via WHAN diagram. In this case we can also see that both ways of determining the galaxy type obtain different results except for the HII Region .

From these results we can conclude that both methods for the classification of galaxies are consistent only for the Star Forming galaxies. On the other hand, when determining

the AGN we find that the two criteria differ and don't predict the same type of galaxy in most of cases.

4.2 Comparison between the Nucleus and the Whole Galaxy

The diagrams obtained from integrated spectra of the whole galaxies is shown in figure (4.6).

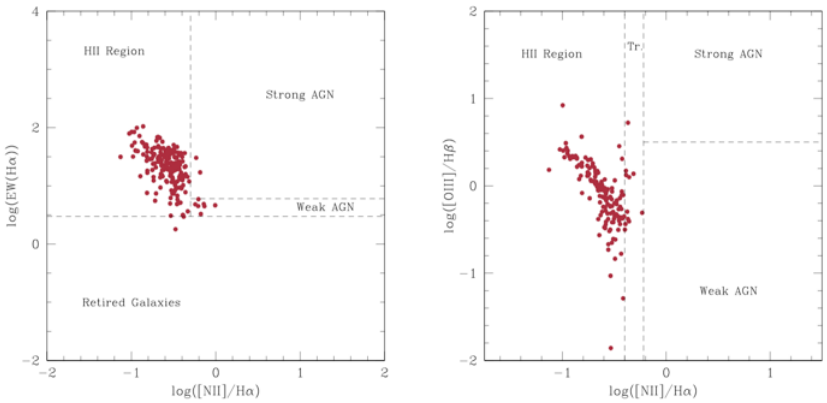

Figure 4.6: BPT (left) and WHAN (right) diagrams with the emission lines taken from the Boselli's Survey.

The figure (4.7) compares the integrated spectra of the whole galaxy superimposed to the nuclear spectra.

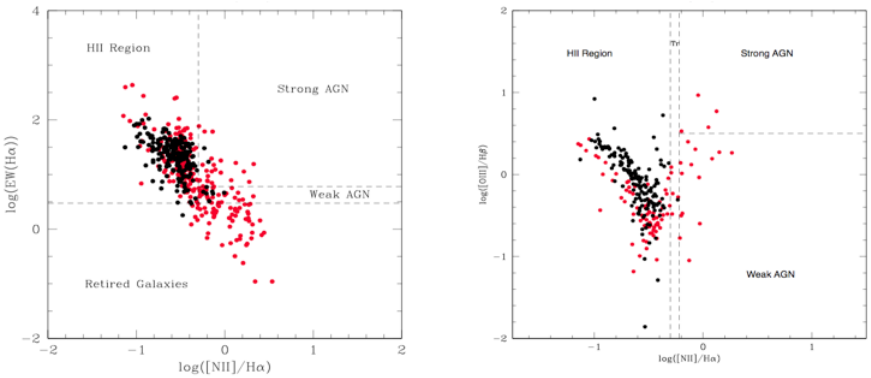

Figure 4.7: BPT (left) and WHAN (right) diagrams with the emission lines taken from the Boselli's Survey superimposed to the nuclear ones. Red dots represent the nucleus and black whole galaxy. Only the nuclear spectra corresponding to galaxies which also have an integrated one have been plotted, so that the quantity of black and red dots is the same.

The next step is to study how the nuclear spectra corresponding to every type of changes when taking the integrated one of the whole galaxy. Similarly to the figures (4.2) and (4.3) where we compared the BPT and WHAN diagrams, the figure (4.6) shows how the spectra change when passing from nuclear spectra to one of the whole galaxy.

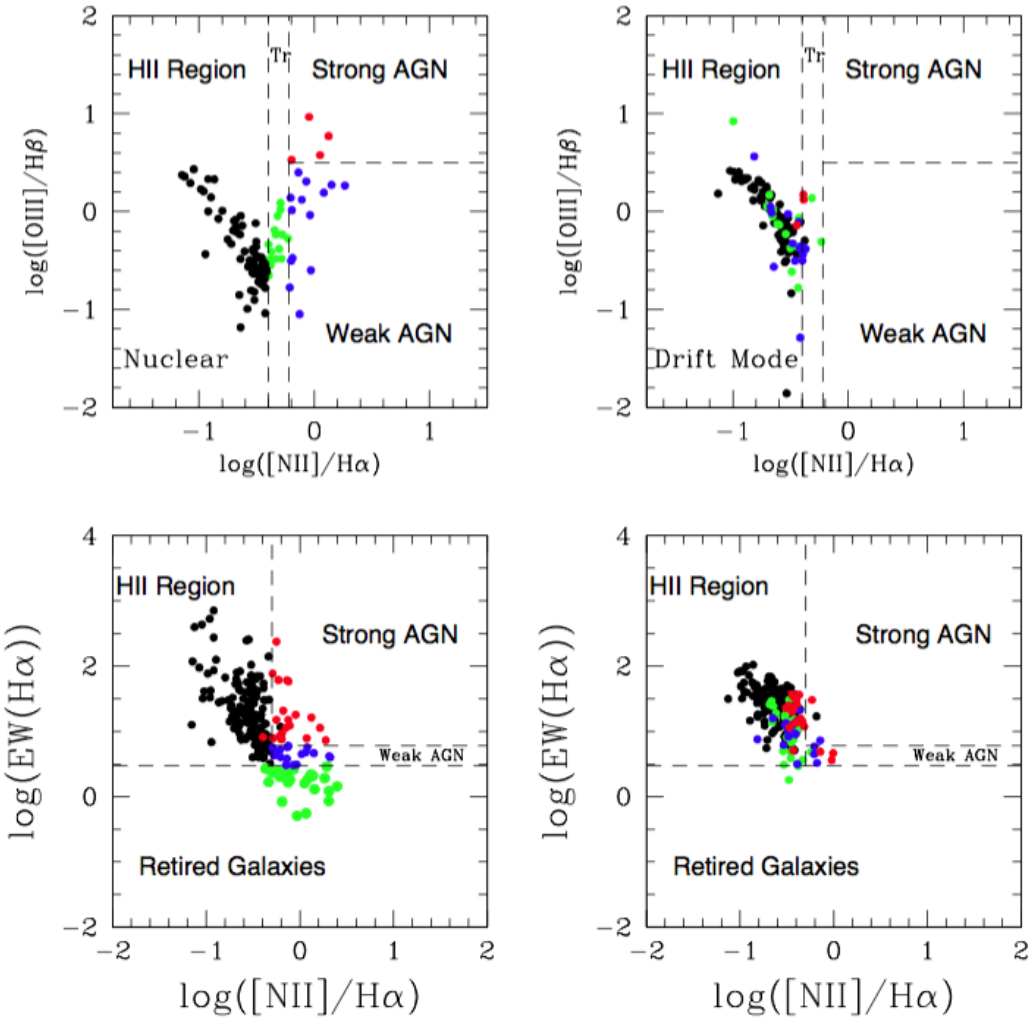

Figure 4.8: Illustration of how do the spectra move from the nucleus to the whole galaxy using the BPT (top) and WHAN (bottom) diagrams. The color of the dots is determined according to the diagram on the left and maintained on the right side, so that it is possible to see the trajectory from one to the other image.

As the same way as done before with the comparison between BPT and WHAN diagrams, the following tables quantifies the results.

BPT				
Nuclear Spectra	**Integrated Spectra of the Whole Galaxy**			
	Strong AGN	*Weak AGN*	*Transition*	*HII Region*
Strong AGN (4) →	0	0	2 (50%)	2 (50%)
Weak AGN (14) →	0	0	3 (22%)	11 (78%)
Transition (15) →	0	0	3 (20%)	12 (80%)
HII Region (65) →	0	0	1 (1.5%)	64 (98.5%)

WHAN				
Nuclear Spectra	**Integrated Spectra of the Whole Galaxy**			
	Strong AGN	*Weak AGN*	*Retired*	*HII Region*
Strong AGN (22) →	1 (4.5%)	3 (13.5%)	0	18 (82%)
Weak AGN (18) →	1 (5.5%)	3 (16.5%)	0	14 (78%)
Retired (27) →	0	1 (3.7%)	2 (7.4%)	24 (88.9%)
HII Region (151) →	1 (0.7%)	0	0	150 (99.3%)

Although the they are not considered in this classifications, the 22 *passive galaxies* in the nucleus remain passive when checking the integrated spectra of the whole galaxy.

These results are also represented graphically in figure 4.9.

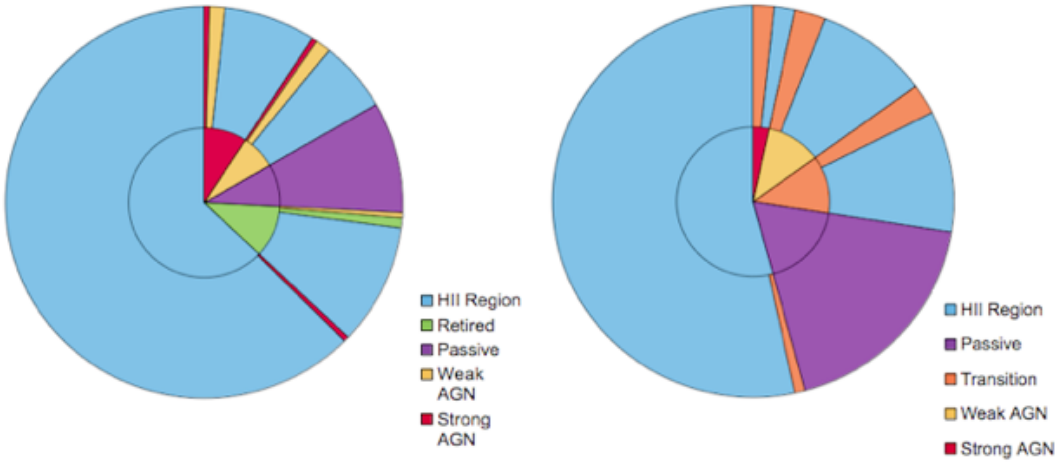

Figure 4.9: Comparison of the classification taking the nuclear and whole galaxy spectra via WHAN (left) and BPT (right) diagrams. The center illustrates the proportion of different kind of galaxies in the nucleus, and in the outer region it is represented how this types move when taking the integrated spectra of the whole galaxy.

It is clear that most significant effect of taking into account the whole galaxy is that most of the galaxy become Star Forming, indicating that in the outer region of the galaxies there is an important amount of star formation.

Chapter 5

Conclusions

We have taken the nuclear spectra of all the 323 galaxies of the *Herschel Reference Sample* from the SDSS, NED and Observatory of Loiano and extract the equivalent widths of the $[OIII]$, $[NII]$, H_α and H_β (except for those galaxies taken at Loiano's Observatory where the used filter didn't cover all the visible region of the spectra so that $[OIII]$ and H_β couldn't be observed).

This data allowed us to introduce the galaxies in the WHAN and BPT diagrams and to make the corresponding classifications. Afterwards we made a comparison of both methods to classify and see if they tend to predict the same galaxy type.

This clearly happens when determining a *HII Region*. In fact in our sample the 100% of the the Star Forming Galaxies classified by BPT also were for WHAN and, inversely, the 89.5% of those determined via WHAN were also SF for BPT. However, when we focused on AGN we realize that both criteria contradict to each other.

It would be reasonable assume that the BPT diagram is more reliable since it takes into account more emission lines.

On the other hand, we have use these results to make a comparison between the spectra of the nucleus and the whole galaxy. The spectra and the emission lines of the whole galaxies were taken from the *Boselli A. et al. (2013)*.

The most obvious and significant conclusion when comparing the BPT or WHAN diagrams is that when passing from the nuclear to the whole galaxy's spectrum there is a big shift to the *HII Region*, i.e. most of the galaxies become Star Forming when taking all the galaxy into account. It indicates that in the outer region of galaxies there is an important amount of ongoing star formation that cannot be ignored.

Another important result is can be seen in the comparison of the WHAN diagram: most of the *Retired Galaxies* become Star Forming (88.9%). It means that these galaxies has been Star Forming in the past and, although the nucleus is sterilized, there are still remnants of star formation in the outer region.

This is, therefore, a very different case compared to the *Passive Galaxies*, given that all of them remain Passive when evaluating the whole galaxy.

From these results it is clear that it's not possible to take the nuclear spectra and consider it as a valid sample of the whole galaxy's one. Moreover, we also deduce that *Aperture Correction* developed in the *Brinchmann et al (2004)* fails since it can't predict a Star Forming galaxy from a nucleus without Hydrogen.

Bibliography

[1] G. Gavazzi, A. Zaccardo, G. Sanvito, A. Boselli, C. Bonfanti, (2004), *Spectrophotometry of galaxies in the Virgo cluster.II: The data*

[2] L.J. Kewley, B. Groves, G. Kauffmann, T. Heckman, (2006), *The host galaxies and classification of active galactic nuclei*

[3] R.C. Fernandes, G.Stasinska, A. Mateus, N.V. Asari, (2011), *A comprehensive classification of galaxies in the Sloan Digital Sky Survey: how to tell true from fake AGN?*

[4] A. Boselli, S. Eales, L.Cortese, G. Bendo, P. Chanial, V. Buat, et al., (2010), *The Herschel Reference Survey*

[5] R. Gualandi, R. Merighi, (2001), *BFOSC (Bologna Faint Spectrograph and Camera) Manuale utente*

[6] G. Gavazzi, G. Savorgnan. M. Fumagalli, (2011), *The complete census of the optically selected AGNs in the Come Supercluster: the dependence of AGN activity on the local environment*

[7] Taylor, (2010), *Introduzione all'analisi degli errori*, Zanichelli

[8] Binney Tremaine, (2008), *Galactic Dynamics*, Princeton

[9] Cid Fernandes, R.; Stasiska, G.; Mateus, A.; Vale Asari, N. (2011), *A comprehensive classification of galaxies in the Sloan Digital Sky Survey: how to tell true from fake AGN?*

[10] Boselli, A.; Hughes, T. M.; Cortese, L.; Gavazzi, G.; Buat, V. (2013), *Integrated spectroscopy of the Herschel Reference Survey. The spectral line properties of a volume-limited, K-band-selected sample of nearby galaxies*

[11] John Moustakas and Robert C.Kennikutt, Jr. (2006), *An integrated spectrophotometric survey of nearby star-forming galaxues*

[12] J. Brinchmann, S. Charlot, S. D. M. White, C. Tremonti G. Kauffmann, T. Heckman and J. Brinkmann (2004), *The physical properties of star-forming galaxies in the low-redshift Universe*

[13] Luis C. Ho AND Alexei V. Filippenko (1997), *A search Dwarf Seyfert Nuclei. III. Spectroscopic parameters and propierties of the host galaxies*